Earth-Science Reviews 155 (2016) 172–197

Contents lists available at ScienceDirect

Earth-Science Reviews

journal homepage: www.elsevier.com/locate/earscirev

Multiproxy assessment of Holocene relative sea-level changes in the western Mediterranean: Sea-level variability and improvements in the definition of the isostatic signal

Matteo Vacchi [a], Nick Marriner [b], Christophe Morhange [a], Giorgio Spada [c], Alessandro Fontana [d], Alessio Rovere [e]

[a] Aix-Marseille Université, CEREGE CNRS-IRD UMR 34, Europole de l'Arbois BP 80, 13545 Aix-en-Provence, Cedex 4, France
[b] CNRS, Chrono-Environnement UMR 6249, Université de Franche-Comté, UFR ST, 16 route de Gray, 25030 Besançon, France
[c] Università degli Studi di Urbino, Dipartimento di Scienze Pure ed Applicate (DiSPeA), Via Santa Chiara 27, Urbino, Italy
[d] Università degli Studi di Padova, Dipartimento di Geoscienze, Via Gradenigo 6, Padova, Italy
[e] University of Bremen, Marum, ZMT, Bremen, Germany

ARTICLE INFO

Article history:
Received 10 July 2015
Received in revised form 3 February 2016
Accepted 12 February 2016
Available online 22 February 2016

Keywords:
Mediterranean Sea
Holocene
Sea-level database
Isostatic adjustment
Sea-level proxy

ABSTRACT

A review of 917 relative sea-level (RSL) data-points has resulted in the first quality-controlled database constraining the Holocene sea-level histories of the western Mediterranean Sea (Spain, France, Italy, Slovenia, Croatia, Malta and Tunisia). We reviewed and standardized the geological RSL data-points using a new multi-proxy methodology based on: (1) modern taxa assemblages in Mediterranean lagoons and marshes; (2) beachrock characteristics (cement fabric and chemistry, sedimentary structures); and (3) the modern distribution of Mediterranean fixed biological indicators. These RSL data-points were coupled with the large number of archaeological RSL indicators available for the western Mediterranean. We assessed the spatial variability of RSL histories for 22 regions and compared these with the ICE-5G (VM2) GIA model. In the western Mediterranean, RSL rose continuously for the whole Holocene with a sudden slowdown at ~7.5 ka BP and a further deceleration during the last ~4.0 ka BP, after which time observed RSL changes are mainly related to variability in isostatic adjustment. The sole exception is southern Tunisia, where data show evidence of a mid-Holocene high-stand compatible with the isostatic impacts of the melting history of the remote Antarctic ice sheet.

Our results indicate that late-Holocene sea-level rise was significantly slower than the current one. First estimates of GIA contribution indicate that, at least in the northwestern sector, it accounts at least for the 25–30% of the ongoing sea-level rise recorded by Mediterranean tidal gauges. Such contribution is less constrained at lower latitudes due to the lower quality of the late Holocene index points. Future applications of spatio-temporal statistical techniques are required to better quantify the gradient of the isostatic contribution and to provide improved context for the assessment of 20th century acceleration of Mediterranean sea-level rise.

Contents

E-mail address: vacchi@cerege.fr (M. Vacchi).

http://dx.doi.org/10.1016/j.earscirev.2016.02.002
0012-8252/

1. Introduction

Relative sea-level (RSL) changes since the Last Glacial Maximum (LGM, ~30 to ~20 ka BP) primarily document the transfer of ice mass from the continents to the oceans during deglaciation (e.g. Peltier and Fairbanks, 2006; Deschamps et al., 2012). Approximately 50 million km^3 of ice have melted from land-based ice sheets, raising RSL in regions distant from the major glaciation centers (far-field sites) by ~135 m (e.g. Bard et al., 1996, 2010; Lambeck and Purcell, 2005; Lambeck et al., 2014). During the Holocene (the last ~12 ka BP), empirical studies and Glacial Isostatic Adjustment (GIA) models show that the rate of ice-mass transfer decreased significantly at ~7 ka BP, when the Earth entered into a period of near RSL stability, after which time the ocean volume changed by just a few meters (e.g. Mitrovica and Milne, 2002; Lambeck et al., 2014).

On a regional scale, the interplay of glacio- and hydro-isostatic processes plays a significant role in defining the Holocene RSL changes. However, other factors have influenced RSL histories as well. Vertical tectonic displacements often appear to be continuous and gradual over time, but frequently consist of large movements, for instance during earthquakes of great magnitude (e.g. Pirazzoli et al., 1994; Nelson et al., 1996; Dura et al., 2014) or volcanic activity (e.g., Morhange et al., 2006). Local factors include modifications of the tidal regime (e.g., Hall et al., 2013) and sediment consolidation due to the accumulation of overlying material and land reclamation (e.g., Törnqvist et al., 2008; Marriner et al., 2012a).

Databases of RSL have been developed to better understand these forcing mechanisms of sea-level change, to identify regional variations and to constrain geophysical models of glacial isostasy (e.g., Engelhart and Horton, 2012; Shennan et al., 2012; Khan et al., 2015).

For the Mediterranean, regional compilations of sea-level data have been produced for both the eastern and the western Mediterranean (e.g., Lambeck and Bard, 2000; Vött, 2007; Lambeck et al., 2004a; Antonioli et al., 2009; Vacchi et al., 2014). These studies used a variety of observational sea-level data from different geomorphic settings and archeological sites to produce RSL data-points. However, a standardized methodology for the production of sea-level index and limiting points (cf. Gehrels and Long (2007); Hijma et al. (2015)) is presently lacking for the Mediterranean region.

In this paper, we reconsidered and reanalyzed the published sea-level data for the western Mediterranean seaboard following the protocol described by the International Geoscience Programme (IGCP) projects 61, 200, 495 and 588 (e.g., Preuss, 1979; van de Plassche, 1982; Gehrels and Long, 2007; Shennan et al., 2015).

Here we present: i) a standardized methodology to produce sea-level index and limiting points from published data deriving from the Mediterranean and ii) a comprehensive database of index and limiting points from 14 ka BP to present, for 22 areas in the western Mediterranean (Fig. 1).

After summarizing the previous studies and reporting the unresolved issues regarding relative sea level in the western Mediterranean (Section 2), we outline the reasons for grouping sea-level data into 22 regions (Section 2.2). We then explain our methodology to produce sea-level index and limiting points (Section 3) and how we predicted the RSL models using the open source numerical code SELEN (Section 4). In Section 5, we reconstruct the RSL histories of the 22 regions using quality controlled sea-level index and limiting points. We then discuss the applicability of our multiproxy approach in the Mediterranean (Section 6.1), we compare and contrast the reconstructed RSL histories with the predicted RSL models (Section 6.2) and, finally, we assess the spatial variability of late Holocene RSL changes in the western Mediterranean providing new insights about the influence of the isostatic contribution on the current sea-level rising rates (6.3).

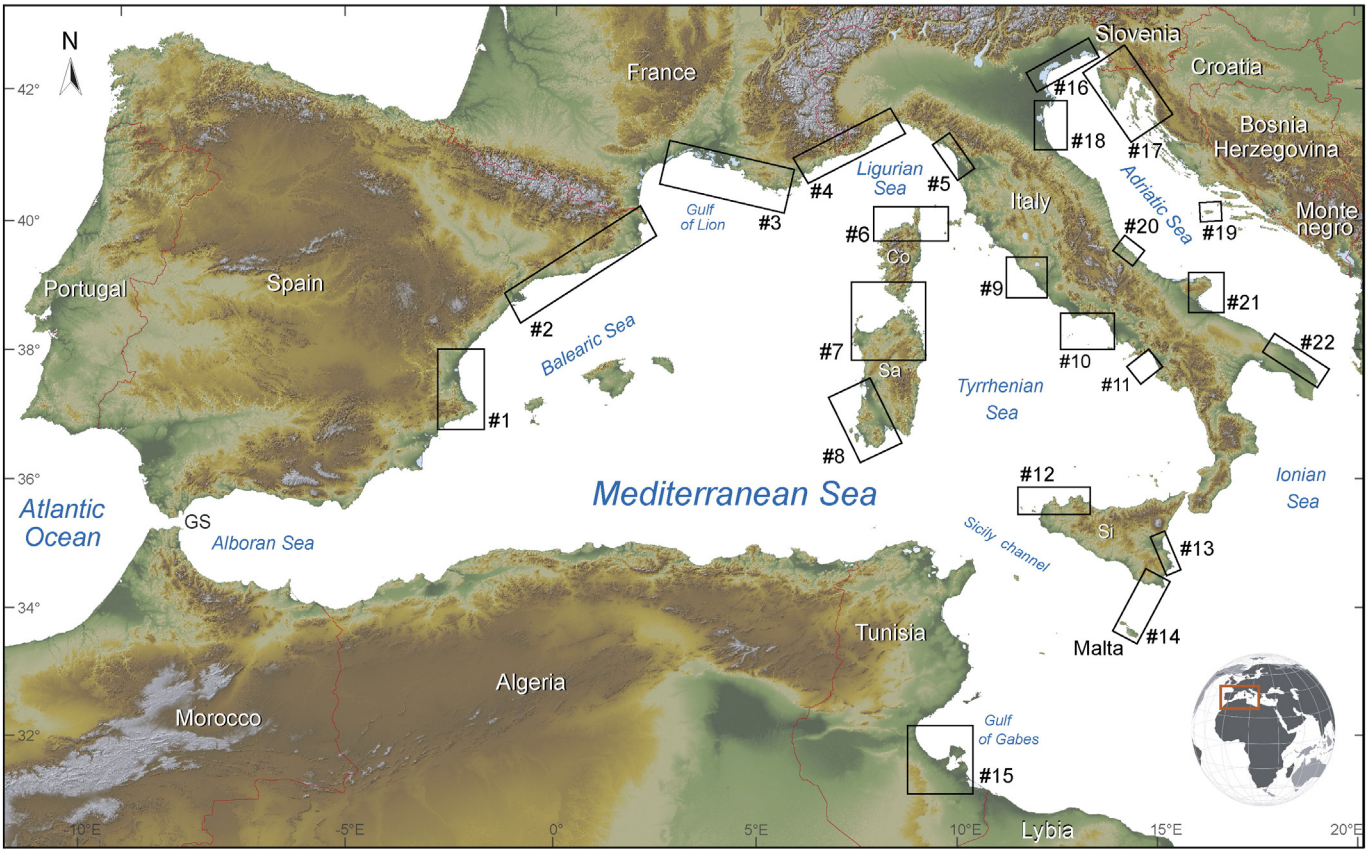

Fig. 1. Spatial extent of the study area. Numbered rectangles denote the location of sea-level data for this paper, grouped into regions as explained in the text. GS is Gibraltar Strait, CO is Corsica, SA is Sardinia, SI is Sicily.

2. Study area

The study area encompasses the western Mediterranean coast at latitudes comprised between 45.7°N and 33°N and longitudes comprised between −0.3°E and 16.2°E (Fig. 1). The data were collected in central and northern Spain, southern France and Corsica, much of the Italian coast (including Sicily and Sardinia), Malta, Slovenia, northern and central Croatia and southern Tunisia (Fig. 1).

Western Mediterranean tides have an average amplitude of about 0.4 m, although they do show spatial variability based on coastal geometry and bathymetry (Tsimplis et al., 1995; Antonioli et al., 2015). Tidal amplitude is very small near the amphidromic points but it may reach amplitudes of up to 2 m in the Gulf of Gabes and the North Adriatic Sea (Tsimplis et al., 1995; Marcos et al., 2009). Around the Straits of Gibraltar, the Atlantic Ocean affects Mediterranean tides in the Alboran Sea (Fig. 1), but its influence rapidly declines further east (e.g., Marcos et al., 2009). Three main deltas, the Ebro, the Rhone, and the Po, represent the main sedimentary inputs into the western Mediterranean basin (Maselli and Trincardi, 2013; Anthony et al., 2014).

From a geological point of view, the western Mediterranean is a tectonically complex area where two small oceanic basins (the Tyrrhenian and Liguro-Provençal back-arc basins) occur along the Nubia–Eurasia convergent margin and are separated by the Corsica–Sardinia rigid continental block (Fig. 2, Jolivet and Faccenna, 2000; Jolivet et al., 2008; Faccenna et al., 2014).

In the western Mediterranean, some parts of the back-arc basin margins are undergoing compressional tectonics (e.g., Billi et al., 2011). This tectonic regime is particularly active, from west to east, along the east-Alboran, Algerian, and south-Tyrrhenian margins (Billi et al., 2011; Faccenna et al., 2014; Fig. 2). In the central Mediterranean, the contractional orogen swings around the Adriatic Sea and marks the deformed margins of Adria (Fig. 2).

2.1. Original source of the data

The post-LGM RSL changes in the western Mediterranean have been investigated since the late 1960s (e.g., Flemming, 1969; Pirazzoli, 1976; Lambeck and Bard, 2000; Lambeck et al., 2004a; Pirazzoli, 2005; Antonioli et al., 2009; Anzidei et al., 2014). In particular, several studies have focused on the late Holocene (last 4 ka) using geo-archaeological archives to reconstruct past sea-level histories in areas of Spain (e.g., Carmona-González and Ballester, 2011), France (e.g., Morhange et al., 2001, 2013), Sardinia (e.g., Antonioli et al., 2007; Orrù et al., 2011, 2014), Croatia (e.g., Antonioli et al., 2007; Faivre et al., 2010), Tunisia (e.g., Anzidei et al., 2011), Sicily (e.g., Scicchitano et al., 2008) and Malta (e.g., Marriner et al., 2012b; Furlani et al., 2013). One of the main goals of the geoarcheological studies has been to establish the RSL histories during the first millennium BC (e.g., Pirazzoli, 1976; Morhange et al., 2001; Lambeck et al., 2004b; Goiran et al., 2009; Evelpidou et al., 2012). In Marseille's ancient harbor, Morhange et al. (2001), coupled geoarcheological and biological sea-level data to reconstruct RSL changes since the Bronze Age. They proposed that RSL was at ~−1.5 m in the Middle Bronze Age (~3.6 ka BP) and ~−1.2 m in the Late Bronze Age (~2.8 ka BP). Between the Archaic and Roman periods (~2.0 to 1.5 ka BP), RSL ranged between −0.8 and −0.4 m with respect to the current Mean Sea Level (MSL).

An ongoing debate concerns the archeological interpretation of ancient Roman fish-tanks (*piscinae*), with implications for the reconstruction of RSL during the Roman period. These coastal structures are assumed to be among the most reliable archeological RSL indicators (Lambeck et al., 2004b; Auriemma and Solinas, 2009; Morhange and Marriner, 2015) because sea level and fish-tank architecture are closely correlated and their chronology is well constrained to between ~1st century BC (~2.1 ka BP) and ~1st century AD (~1.9 ka BP).

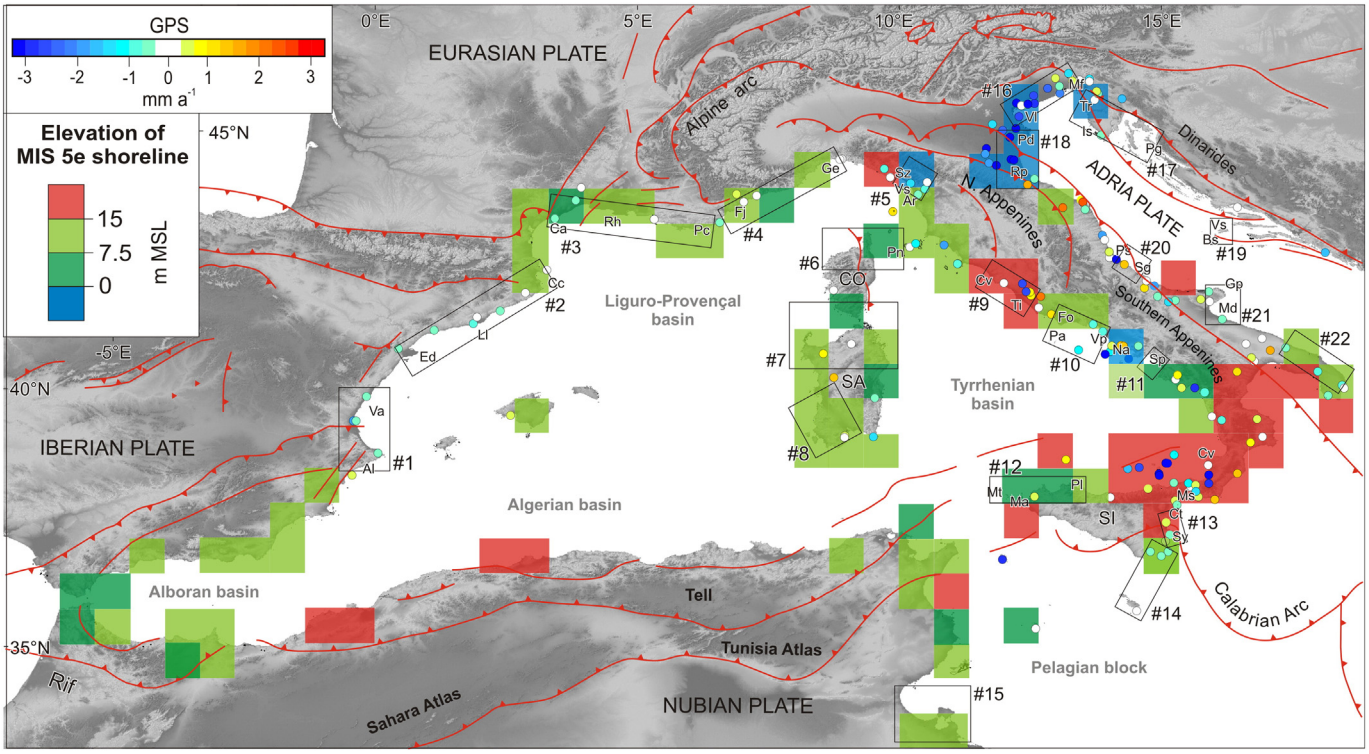

Fig. 2. Tectonic framework of the western Mediterranean. Faults are modified after Faccenna et al. (2014). Squares indicate the average elevation of MIS 5e shorelines (data from Ferranti et al. (2006); Pedoja et al. (2014)). Dots denote the ongoing GPS-derived vertical movements along the Mediterranean coast (data from Serpelloni et al. (2013)). CO, Corsica; SA, Sardinia; SI, Sicily. Al, Alicante; Va, Gulf of Valencia; Ed, Ebro Delta; Ll, Llobregat Delta; Cc, Cap Creus; Ca, Cap d'Agde; Rh, Rhone Delta; Pc, Port Cros; Fj, Frejus; Ge, Genova; Sz, La Spezia; Vs, Versilia plain; Ar, Arno river; Pn, Pianosa Island; Cv, Civitavecchia, CV; Ti, Tiber Delta; Fo, Fondi plain; P, Pontine Archipelago; Vp, Volturno plain; Na, Naples volcanic district; Sp; Sele plain; Cv, Capo Vaticano; Ms, Messina Strait; Mt, Marettimo Island; Pl, Capo Gallo; Ma, Marsala sound; Ct, Catania; Sy, Syracuse; Mf, Monfalcone; Vl, Venice lagoon; Pd, Po Delta; Rp, Romagna coastal plain; Ps, Pescara; Sg, Sangro plain; Gp, Gargano promontory; Md, Gulf of Manfredonia.

Lambeck et al. (2004b) reported an extensive analysis of fish tanks in the Tyrrhenian Sea, and calculated Roman RSL at ~−1.3 m MSL. The archaeological interpretation was based on both field surveys and on the analysis of original Latin descriptions. Important features in the fish-tank architecture are: i) the sluice gate (*cataracta*) that controlled water exchange between the tanks and the open sea, while not permitting the fish to escape; ii) channels that assured water exchange, sometimes carved into the rocky bedrock; iii) foot-walks (walking surfaces, *crepidines*) delimiting the fish tank basin and generally occurring at two or three levels (Schmiedt, 1972).

Lambeck et al. (2004b) proposed that the upper limit of RSL in Roman times was 0.2 m below the lowest walking surface (*crepido*). Lambeck et al. (2004b) and subsequently Auriemma and Solinas (2009) suggested that the flow of water inside the fish tanks was tidally controlled by the paleo mean lower water denoted by the channel thresholds, often corresponding to the base of the mobile *cataracta*. Such an archeological interpretation has since been applied to a number of other coastal areas in the western Mediterranean (e.g., Antonioli et al., 2007, 2011; Anzidei et al., 2011).

Evelpidou et al. (2012) also performed a detailed survey of the Tyrrhenian Sea's fish tanks proposing that RSL in the Roman period ranged between ~−0.6 and ~−0.3 m MSL. These authors disagreed with the interpretation of an original supratidal position for the lowest *crepido* stating that the height of the *cataracta* proposed by Lambeck et al. (2004b) would not have been sufficient for the fish tanks to function properly. Furthermore, Evelpidou et al. (2012) stated that the channel threshold and the base of the *cataracta* can be located at any depth in the basin and, therefore, they cannot be considered a reliable sea-level indicator. More recently, Morhange et al. (2013) used the palaeobiological zoning of fixed marine fauna inside a Roman fish tank at Frejus (France) to infer RSL at that time. They suggested that, at Frejus, the fixed gates were built in subtidal position and were positioned at least 0.3 m below the upper limit of in situ fixed marine organisms (*Serpulidae* spp, *Cladocora caespitosa* and *Ostrea* spp.).

In contrast to the late Holocene, there is comparatively less data for early to mid-Holocene RSL changes in the western Mediterranean. Lambeck and Bard (2000), compiled a comprehensive assessment of RSL variations in southern France for the last 30 ka BP. Similarly, Correggiari et al. (1996), Lambeck et al. (2004a, 2011) and Antonioli et al. (2009) assessed the postglacial RSL changes along the Italian peninsula and Croatia. RSL history since the mid-Holocene has been investigated in France (e.g., Laborel et al., 1994; Vella and Provansal, 2000), Tunisia (e.g., Jedoui et al., 1998; Morhange and Pirazzoli, 2005), Corsica and Sardinia (e.g., Laborel et al., 1994; Antonioli et al., 2007). Significant sea-level data have also been collected as part of coastal investigations with other purposes, for example, studies of Holocene environmental changes in marshes and coastal lagoons in Spain (e.g., Dupré et al., 1988; Marco-Barba et al., 2013), France (e.g., Raynal et al., 2010; Sabatier et al., 2010), Sardinia (e.g., Di Rita and Melis, 2013; Orrù et al., 2014), Tunisia (e.g., Lakhdar et al., 2006; Zaîbi et al., 2011) as well as along the Adriatic (e.g., McClennen and Housley, 2006; Caldara and Simone, 2005) and Tyrrhenian (e.g., Di Rita et al., 2010; Sacchi et al., 2014) coasts of Italy.

We further used sea-level data provided by studies focused on neotectonics and paleo-tsunami impacts in Sicily (e.g., De Martini et al., 2010; Gerardi et al., 2012) and along the Adriatic coast (e.g., Furlani et al., 2011; Marriner et al., 2014). Other coastal studies with sea-level data have focused on the sedimentary evolution of large deltas (e.g., Somoza et al., 1995; Vella et al., 2005; Amorosi et al., 2008a) and other major coastal plains (e.g., Dubar and Anthony, 1995; Rossi et al., 2011; Milli et al., 2013). Finally, we extracted sea-level data from cores undertaken within the framework of the recently updated Italian Geological Maps (e.g. Cibin and Stefani, 2009; Sarti et al., 2009).

2.2. Database subdivision

To account for the spatial variability of RSL changes we divided the database into 22 regions (Figs. 1 and 2) on the basis of (1) geographical position, (2) proximity to other RSL data-points (commonly a function of local geomorphology, such as coastal plains between headlands, (Engelhart et al., 2015), and (3) the regional neotectonic setting derived from the elevation of the last interglacial shoreline (MIS 5e, data from Ferranti et al., 2006, 2010; Pedoja et al., 2014, if not otherwise specified, Fig. 2) and, secondarily, from the ongoing GPS-derived vertical velocities (data from Serpelloni et al. (2013), Fig. 2).

Probabilistic assessment suggests that sea-level elevation during the last interglacial (~125 ka ago) was ~7.2 m above the present MSL (Kopp et al., 2009). In Fig. 2, the dark and pale green boxes (50 km^2 squares) show the average elevation of the MIS 5e shoreline (as reported by Ferranti et al., 2006; Pedoja et al., 2014). Dark green boxes indicate average elevation of between 7.5 and 15 m (stable to very minor uplift) while pale green indicates elevation between 0 and 7.5 m (stable to very minor subsidence). These regions can be considered as being affected by a long-term vertical movement of between −0.06 and +0.06 mm a^{-1}, averaged for the last ~125 ka. It is worth highlighting that such vertical rates include both tectonics and the GIA signal (Dutton and Lambeck, 2012), and that uplift/subsidence rates are probably not linear over the last 125 Ka.

In order to better understand the current vertical movements, we also analyzed ongoing vertical movements recorded by GPS. Discrepancies between long-term vertical velocities and GPS measurements were elucidated for some regions. Western Mediterranean GPS trends are based on short records (often less than 15 years, Serpelloni et al., 2013). Thus, they can give insights into the on-going vertical movements but are less representative of the general vertical trend of a given region with respect to the MIS 5e elevation. For this reason, we primarily used the long-term vertical velocities provided by the elevation of the last interglacial shoreline for the subdivision of our database

We subdivided the Spanish Mediterranean coast into two regions (Figs. 1 and 2). Central Spain (#1) extends between Alicante and the Gulf of Valencia and represents the westernmost region in our database. In this area, historical seismicity is reported (Olivera et al., 1992). GPS vertical velocities document a general subsidence trend with rates lower than 2 mm a^{-1} in this region, notably in the Gulf of Valencia. The northern Spanish coast (#2) extends from the Ebro Delta to Cap Creus, at the border with France (Fig. 2). GPS-derived vertical velocities indicate zero vertical motion in most of the regions, with the exception of the Ebro and Llobregat deltas that show subsidence of 1.5 mm a^{-1}.

The central French coast extends from Cape d'Agde to Port Cros Island, including the Rhone Delta. GPS-derived vertical velocities suggest zero ongoing vertical motion. The elevation of MIS 5e shorelines denotes a long-term stability of the area (Ambert, 1999).

We subdivided the northern coast of the Ligurian Sea into two regions (Figs. 1 and 2). The western Ligurian Sea (#4) encompasses the coastline between Frejus (France) and Genoa (Italy). Nonetheless, although both MIS 5e and GPS-derived velocity fields indicate negligible vertical movement across the whole area (Fig. 2), Dubar et al. (2008) documented a mild uplift (up to 0.06 mm a^{-1}) around the overthrusting Nice Range on the basis of the local MIS 5e elevation.

The eastern Ligurian sea region (#5) stretches from La Spezia to the Arno river coastal plain (Fig. 2). Both GPS and long-term vertical velocities indicate a general subsidence trend of this region, with rates of up to ~0.26 mm a^{-1} on the Versilia coastal plain.

Corsica and Sardinia show a general tectonic stability since the last interglacial (Ferranti et al., 2006; Fig. 2). They occupy the central sector of the western Mediterranean, and they were subdivided into the following three regions, northern Corsica and Pianosa, (#6), southern Corsica-Northern Sardinia (#7) and southwestern Sardinia (#8) according to the geographical distribution of the data. Sea-level data from Pianosa Island were included in region (#6) due to its proximity to northern Corsica (Fig. 2). GPS-derived vertical velocities indicate zero to weakly positive on-going vertical motion in the three regions (Fig. 2). The north-central Latium region (#9) stretches from Civitavecchia to the Tiber Delta (Figs. 1, 2). In this region, GPS-derived vertical velocities range from zero to less than 1 mm a^{-1} while stability to moderate uplift (≤0.23 mm a^{-1}) is documented since the last interglacial. On the Tiber Delta, long-term uplift of ~0.11 mm a^{-1} is reported.

The southern Italian coast presents a very complex tectonic setting (Fig. 2, Ferranti et al., 2010; Faccenna et al., 2014). The Gulf of Gaeta region (#10) stretches from the Fondi to the Volturno coastal plains and includes the Pontine Archipelago (Fig. 2). 0.3 to 0.2 mm a^{-1} of subsidence is reported on the Volturno plain during the last ~40 ky BP. GPS-derived vertical velocities indicate a predominant on-going subsidence across the area, with greater rates in the volcanic district of the Gulf of Naples (−8 mm a^{-1}, Fig. 2) where we avoided the RSL reconstruction. In fact, it would be not indicative of the general RSL trend because this area is strongly affected by significant non-eruptive crustal deformation (Morhange et al., 2006). Salerno Bay (#11) includes the coastal plains of Sele River and is located south of the volcanic district of the Gulf of Naples. The several MIS-5e shorelines found in the area indicate average long-term uplift ≤0.06 mm a^{-1} and no nearby GPS-derived vertical velocities are available.

We have avoided RSL reconstructions from the tectonically-active Calabrian arc, (Fig. 2) which has been affected by significant tectonic uplift since the last interglacial (Dumas et al., 2005; Ferranti et al., 2006, 2007). The highest rates of uplift are reported near Capo Vaticano (0.6 to 2 mm a^{-1} Tortorici et al., 2003; Ferranti et al., 2010) and in the Messina Straits (~1.0–1.4 mm a^{-1}) between Calabria and Sicily (Fig. 2). This uplift pattern is related to the interplay between regional and local (i.e. fault related) components of vertical displacement (e.g., Ferranti et al., 2007; Scicchitano et al., 2011); rates of uplift decrease progressively southwards and westwards of the Messina Strait (Ferranti et al., 2010). We have subdivided the coasts of Sicily and Malta into three regions (Figs. 1, 2). The northwestern Sicily region (#12) stretches from Palermo to Marsala, including Marettimo Island. The region shows ongoing vertical movements ≤0.4 mm a^{-1} and is considered to have been tectonically stable since the last interglacial. The mid-eastern Sicily region (#13) stretches from Catania to Syracuse. In this area, long-term uplift rates range between 0.4 and 0.7 mm a^{-1} (Dutton et al., 2009; Spampinato et al., 2011) and GPS data indicate on-going uplift ≤1 mm a^{-1} decreasing southwards. In this area, large earthquakes and associated tsunamis have been recorded since historical times (Scicchitano et al., 2007; De Martini et al., 2010).

Even if they are separated by about 100 km of sea, we grouped the southernmost part of Sicily and the Maltese Islands into a single region (#14). These two sectors present zero to minimal ongoing vertical movement (Fig. 2) and very weak historical seismicity is reported for the area. The relatively shallow (≤−200 m) Malta Plateau presently divides these two coastal sectors, which were probably connected during the LGM (Micallef et al., 2013). Pedley (2011) reported the long-term tectonic stability of the Maltese Islands.

The southern Tunisia region (#15) represents the southernmost area of our database (Figs. 1 and 2). No significant historical seismicity is reported in the region and several studies have underlined the tectonic stability of southeastern Tunisia since the MIS 5e (Fig. 2, Jedoui et al., 1998).

We subdivided the northern Adriatic Sea into three regions (Figs. 1 and 2). The lagoons of Venice and Friuli, (#16) stretch from the town of Venice to the town of Monfalcone including three large coastal lagoons (Venice, Caorle and Grado-Marano); a long-term subsidence trend, ranging between 0.7 and 0.4 mm a^{-1} (Carminati et al., 2003; Amorosi et al., 2008b), is reported in this region. GPS-derived data also indicate a subsidence trend with rates higher than 2.5 mm a^{-1} (Fig. 2). The northeastern Adriatic region (#17) encompasses the Gulf of Trieste (Italy and Slovenia) as well as the Istrian coast and the Island of Pag (Croatia). Ongoing vertical movements are lower than

−0.5 mm a^{-1} (Fig. 2), although there is no robust information about the elevation of the MIS 5e coastline in this region. The area is affected by historical seismicity up to M = 6.0 in the southern sector (Herak et al., 1996).

The northwestern Adriatic region (#18) includes the southern part of the Po Delta and the whole Romagna coastal plain. A major subsiding trend is documented across the area since the MIS 5e. High rates, up to 1 mm a^{-1}, occur near the Po Delta decreasing southwards to 0.6 mm a^{-1}. GPS-derived vertical motion also indicates a clear pattern of subsidence, with rates higher than ~3 mm a^{-1} across the whole region.

We subdivided the central and southern Adriatic Sea into four regions. The mid-eastern Adriatic Sea (Figs. 1 and 2; #19) includes data from Vis and Bisevo Islands, located in the eastern part of the central Adriatic Sea, in Croatia. Nearby GPS vertical velocities indicate zero motion. In this region, medium to strong historical seismicity (such as the 1956 M = 5.7 earthquake) is reported (Herak et al., 1996).

The mid-western Adriatic Sea (#20) includes data from the central coast of Abruzzo, between Pescara and the Sangro coastal plain (Figs. 1 and 2). There is a paucity of long-term rates for vertical movements in this region. Furthermore, GPS-derived vertical velocities are contrasting in this region (Fig. 2).

The northern Apulia region (#21) includes the eastern Gargano promontory and the Gulf of Manfredonia (Figs. 1 and 2). To the west, the elevation of the MIS 5e shoreline on the Gargano promontory indicates moderate uplift. Contrasting GPS-derived vertical velocities range from zero movement down to moderate subsidence of ~0.5 mm a^{-1}. The region was historically affected by intense seismicity (Mastronuzzi and Sanso, 2002). As a consequence, the Holocene evolution of some sites on the western Gargano promontory (e.g., the Fortore River coastal plain and the Lesina Lake coastal barrier) have been strongly influenced by strong seismic events which produced co-seismic vertical displacements and devastating tsunamis (Mastronuzzi and Sanso, 2002, 2012). The southern Apulia region (Figs. 1, 2; #22) represents the easternmost areas of our database. Stability to weak subsidence since the last interglacial is reported for this region. This trend is corroborated by nearby GPS-derived vertical velocities.

3. Compilation of the RSL database

3.1. Indicators of former RSL

In order to produce an index point, the following information is required for each RSL indicator: (1) the location of the indicator; (2) the calibrated age of the indicator; and (3) the elevation of the indicator, corrected for the indicative meaning; (i.e. a known relationship between the indicator and a contemporaneous tidal level, the Mean Sea Level (MSL) in our database Shennan et al., 2015; Hijma et al., 2015). The indicative meaning is composed of a reference water level (RWL) and the indicative range (IR). The IR is the elevational range over which an indicator forms and the RWL is the midpoint of this range, expressed relative to the same datum as the elevation of the sampled indicator (e.g., Hijma et al., 2015, Fig. 3). Where a suite of quality controlled sea-level index points exist for a locality or region, they describe changes in RSL through time and can be used to estimate the rates of change. If a sea-level indicator did not show a clear and reasonably established relationship with the MSL, we converted it into a limiting point (see Section 3.2). Although these data are not used to produce sea-level index points, they are extremely important in constraining the RSL above or below the terrestrial or limiting point (e.g., Shennan and Horton, 2002).

Tidal information was obtained from the National and International networks of tidal stations (e.g. IGN-Red de Maréografos, Spain; Service Hydrographique SHOM, France; ISPRA-Rete Mareografica Nazionale; HHI; Hrvatski Hidrografski Institut; Admiralty Tide Tables, UK). Local tidal measurements (e.g. Morhange and Pirazzoli, 2005) or tidal modeling (e.g. Antonioli et al., 2015) were also used.

In the following section we describe the different types of index points used in the database.

3.1.1. Fixed biological index points

Along the western Mediterranean coasts, the coralline rhodophyte *Lithophyllum byssoides* build reef-like bioconstructions just above MSL at the base of the mid-littoral zone (e.g., Pérès and Picard, 1964; Laborel et al., 1994). Its lower limit is defined as the biological mean sea level (i.e. the sharp transition between the midlittoral and the infralittoral zone, Morri et al., 2004), which corresponds to the MSL with reasonable accuracy (≤0.1 m) in microtidal environments (e.g., Stiros and Pirazzoli, 2008; Schembri et al., 2005). *L. byssoides* rims are almost absent in very sheltered areas; they usually develop around the inlets of exposed coasts because the organic construction needs strong mixing of water but moderate wave impact to develop. Fossil rims of *L. byssoides* are accurate proxies for past RSL (e.g., Faivre et al., 2013; Rovere et al., 2015) and have been used for high-resolution (±0.1 to ±0.2 m of vertical uncertainty) RSL reconstructions in southern France and Croatia (e.g., Laborel et al., 1994; Faivre et al., 2013). *L. byssoides* has a very narrow vertical living range and rims form at and slightly above the biological mean sea level (i.e. in the upper midlittoral zone; Laborel and Laborel-Deguen, 1994; Laborel et al., 1994). The indicative range associated with these samples is from the Highest Astronomical Tide HAT to MSL (Fig. 3A, Table 1). The database also includes four samples of fossil Vermetid reefs of *Dendropoma petraeum* collected in Sicily (region #12). The living range of these fixed Gastropoda is quite large (the lower intertidal to the infralittoral zones, Rovere et al., 2015). However, on the basis of the modern distribution of Vermetid reefs measured in Sicily (Antonioli et al., 1999; Lambeck et al., 2004a), we assigned an indicative range of MSL to Mean Lower Water MLW to these samples (Fig. 3A, Table 1). This indicative range cannot be applied to other areas of the Mediterranean without a preliminary measurement of the local distribution of the living Vermetid reefs.

Biological sea-level markers are not perfect horizontal lines but are naturally warped, even over short distances, due to local variations in hydrodynamics and morphology (Stiros and Pirazzoli, 2008; Faivre et al., 2013). For this reason, we added an environmental error of ±0.2 m to the fixed biological indicators included in the database.

3.1.2. Marsh and lagoonal index points

The majority of sea-level index points in previously published sea-level databases are salt-marsh deposits (e.g., Shennan and Horton, 2002; Engelhart and Horton, 2012). However, due to the microtidal regime of the Mediterranean, salt-marsh areas are less developed than on oceanic coastlines and are usually concentrated around large deltas (e.g., Somoza et al., 1998; Vella and Provansal, 2000) and downdrift coastal lagoons (e.g., Silvestri et al., 2005; Marco-Barba et al., 2013).

For salt marshes, the indicative meaning was estimated using the present zonation of vegetation (e.g., Silvestri et al., 2005; Primavera et al., 2011) and microfossil assemblages (e.g., Serandrei-Barbero et al., 2006; Caldara and Simone, 2005). The indicative range associated with samples of salt-marsh origin is from the HAT to MSL (e.g., Hijma et al., 2015, Fig. 3B Table 1). In the Rhone Delta, Vella and Provansal (2000) found that the modern distribution of freshwater peats is between 0.1 and 0.6 m above the current MSL. This indicative range was therefore applied to the samples from the Rhone and the Ebro deltas, which present a similar geomorphic context (Somoza et al., 1998; Vella et al., 2005) and tidal range (Tsimplis et al., 1995).

The remaining freshwater peats of the database were conservatively transformed into terrestrial limiting points (see Section 3.2).

Coastal lagoons are a very common feature of Mediterranean coastlines. They are inland waterbodies, usually developing parallel to the coast, typically separated from the open sea by a sandy barrier

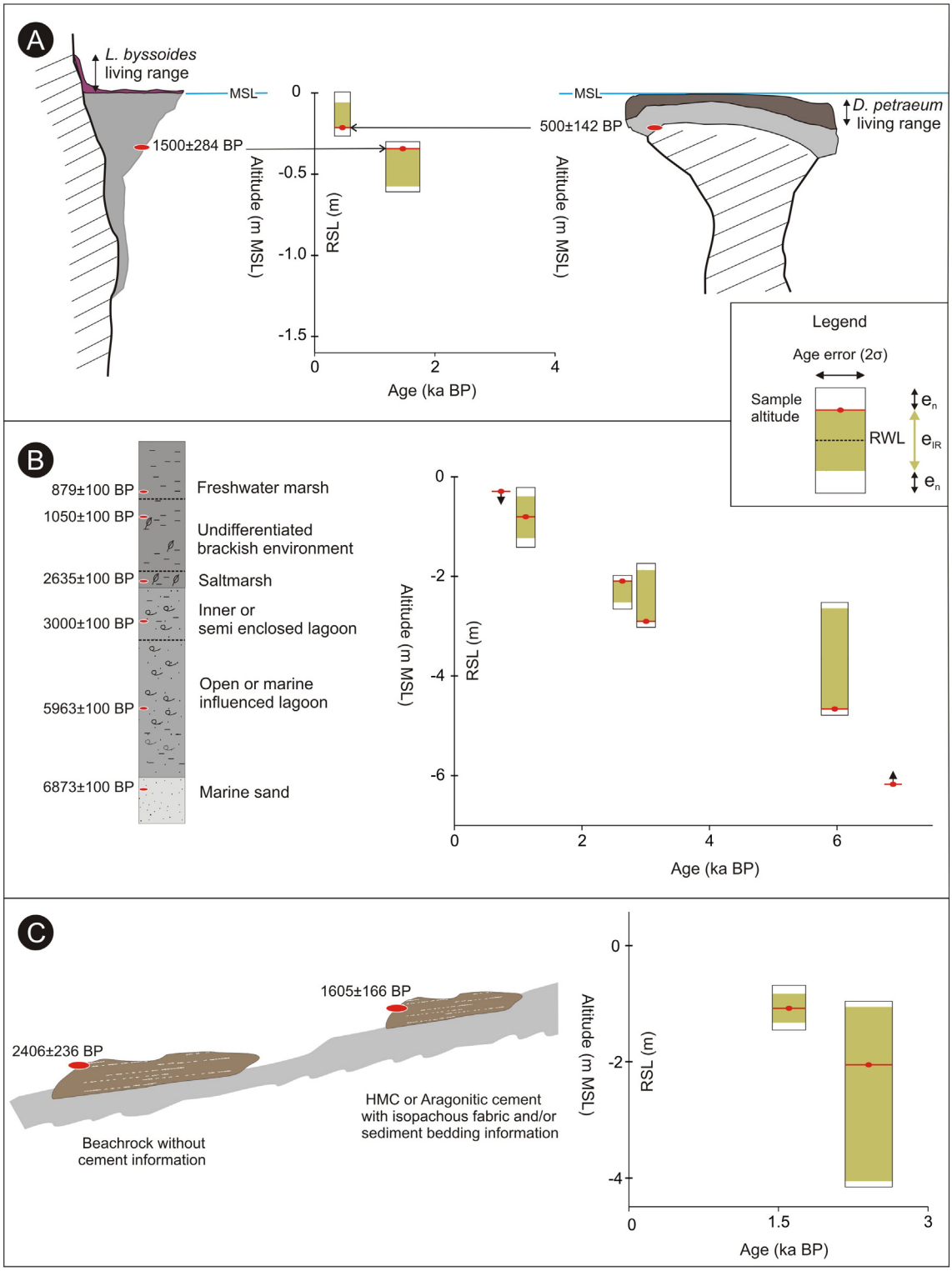

Fig. 3. Schematic diagram of the indicative meaning and theoretical examples of its application in reconstructing RSL from radiocarbon-dated fixed biological samples (A), lagoonal and marsh samples (B) and beachrocks samples (C). RWL is the Reference Water Level, e_{IR} is the indicative range, e_n represents the sum of the error associated with sea level research, HMC is High Magnesium Calcite; MSL is the modern Mean Sea Level.

(e.g., Kjerfve, 1994; Anadón et al., 2002). One or more restricted inlets ensure their continuous or intermittent connection to the open sea. The water depth is generally less than 1 m and seldom exceeds a few meters (e.g., McClennen and Housley, 2006; Marco-Barba et al., 2013; Sacchi et al., 2014).

Modern micro- and macro-fauna (e.g., Ruiz et al., 2005; Carboni et al., 2009; Nachite et al., 2010) and fossil assemblages (e.g. Caldara et al., 2008; Amorosi et al., 2013; Marriner et al., 2012b) define two main types of lagoonal facies in the Mediterranean.

(i) open or marine-influenced lagoon facies are generally characterized by sandy to silty sediments rich in marine brackish molluscs such as *Cerastoderma glaucum* or *Bittium reticulatum*. This facies usually has high species diversity (e.g., Marriner et al., 2012b). Foraminiferal and ostracods assemblages are dominated by marine brackish or outer

Table 1
Summary of the indicative meanings used to estimate the relative elevation of the sea-level index points and limiting points for the database. HAT — Highest Astronomical Tide; MHW — Mean High Water; MLW — Mean Low Water; and MSL — Mean Sea Level. Note that HAT in the Mediterranean is close to the Mean Highest High Water and typically does not exceed 0.1 m above the MHW (exceptions are the Gulf of Gabes and the Northern Adriatic).

Sample type	Evidence	Reference water level	Indicative range
Index points			
Lithophyllum byssoides rim	Identifiable in situ coralline rhodophyte *Lithophyllum byssoides* (formerly known as *Lithophyllum lichenoides*) recognized at species level (Laborel et al., 1994; Faivre et al., 2013).	(HAT to MSL)/2	HAT to MSL
Dendropoma petraeum Vermetid rim	Identifiable in situ Vermetid reefs of *Dendropoma petraeus* recognized at species level (Antonioli et al., 1999; Lambeck et al., 2004a).	(MSL to MLW)/2	MSL to MLW
Salt marsh	Marsh plant macrofossils (e.g. Vella and Provansal, 2000; Silvestri et al., 2005; Serandrei-Barbero et al., 2006; Di Rita et al., 2010). Foraminiferal and diatom assemblages dominated by saltmarsh taxa (e.g., Serandrei-Barbero et al., 2006; Caldara and Simone, 2005; Blázquez and Usera, 2010).	(HAT to MSL)/2	HAT to MSL
Open or marine influenced lagoon	Macrofossil taxa dominated by marine brackish molluscs with the presence of *Cerastoderma glaucum*, *Bittium reticulatum* often associated with *Cerithium vulgatum* and *Loripes lacteus* (e.g. Gravina et al., 1989; Carboni et al., 2010; Di Rita et al., 2011). Foraminiferal and ostracods assemblages dominated dominated by marine brackish littoral taxa (e.g. *Aurila* spp., *Xestoleberis* spp., some species of *Leptocythere*; *Loxoconcha* spp.) or outer estuary taxa (e.g., Mazzini et al., 1999; Carboni et al., 2002; Amorosi et al., 2008b; Ruiz et al., 2006; Rossi et al., 2011; Zaîbi et al., 2011). Higher species diversity compared to the semi-enclosed lagoon system.	−1 m	MSL to −2 m
Inner or semi-enclosed lagoon	Macrofossil taxa dominated by brackish molluscs typical of sheltered marine-lacustrine environments with the presence of *Cerastoderma glaucum*, *Abra segmentum*, Hydrobbiidae spp. (e.g. Caldara et al., 2008; Carboni et al., 2010; Raynal et al., 2010). Foraminifera, diatoms and ostracod assemblages dominated dominated by brackish littoral taxa or inner estuarine taxa (e.g *Cyprideis torosa*, *Leptocythere lagunae*, *Loxoconcha elliptica*, *Cytherois fischeri*; e.g., Amorosi et al., 2009; Nachite et al., 2010; Marriner et al., 2012b; Marco-Barba et al., 2013). Lower species diversity compared to the open lagoon system.	−0.5 m	MSL to −1 m
Undifferentiated brackish environment	Marsh plant macrofossils (e.g. Silvestri et al., 2005; Serandrei-Barbero et al., 2006). Molluscs, foraminiferal, diatoms and ostracods assemblages dominated by freshwater-slightly brackish or swamp taxa and shallow marine taxa (e.g. Colombaroli et al., 2007; Amorosi et al., 2013).	(HAT to MLW)/2	HAT to MLW
Beachrocks with cement fabric or stratigraphic information	Samples showing irregularly distributed needles or isopachous fibres of aragonitic cement or isopachous rims (bladed or fibrous) and micritic HMC cement. Small-scaled trough cross stratification or low angle seaward dipping tabular cross bedding with the presence of keystone vugs (e.g. Strasser et al., 1989; Vousdoukas et al., 2007; Desruelles et al., 2009; Mauz et al., 2015b)	(HAT to MLW)/2	HAT to MLW
General beachrock	Samples that do not meet the above requirements to be classified as strictly intertidal beachrocks	0.5 m	MSL to 2 m and to −1 m
Limiting points			
Marine limiting	In situ infralittoral benthos (e.g. Sartoretto et al., 1996; Rovere et al., 2015). Identifiable marine shells in poorly to well-bedded sandy and silty sediments typical of the upper shoreface or prodelta environments (e.g., Sabatier et al., 2010; Marriner et al., 2012b). *Posidonia oceanica* beds found in open marine deposits. Foraminiferal and ostracod assemblages dominated by marine taxa (Carboni et al., 2002; Zaîbi et al., 2011; Amorosi et al., 2013). Lagoonal sediments that do not meet the above requirements to be classified as index points.	MSL	Below MSL
Terrestrial limiting	Freshwater plant macrofossils and peat with freshwater diatoms (e.g., Colombaroli et al., 2007; Di Rita et al., 2010). Upper beach deposits and terrestrial paleosoils. Foraminiferal and ostracod assemblages dominated by freshwater taxa in swamps or fluvial environnents (Carboni et al., 2002; Milli et al., 2013; Rossi et al., 2011; Amorosi et al., 2013).	MSL	Above MSL

estuary taxa (e.g., *Aurila* spp., *Xestoleberis* spp., *Leptocythere* spp., *Loxoconcha* spp.). Finding a direct relationship between these fossil assemblages and a palaeo MSL is challenging because quantitative analysis of modern analogs are seldom reported in the literature. Nonetheless, we produced index points using samples containing in situ *C. glaucum* mollusc shells, a euryhaline species living in salinities of 4–100‰ and not tolerant of significant aerial exposure (Nikula and Väinölä, 2003; Orrù et al., 2014). Since *C. glaucum* lives within the first 2 m of depth (Gravina et al., 1989; Lambeck et al., 2004a; Primavera et al., 2011), we associated an indicative range from 0 to −2 MSL to the samples in outer or marine-influenced lagoon facies (Fig. 3B, Table 1).

ii) Inner or semi-enclosed lagoon facies show sedimentological and micropaleontological features typical of a brackish lagoonal/estuarine environment with lower species diversity with respect to the open marine facies. There is a dominance of macrofossils typical of sheltered marine-lacustrine environments with the presence of *C. glaucum*, *Abra segmentum*, *Loripes lacteus* and *Hydrobiidae* spp. (e.g., Gravina et al., 1989; Sabatier et al., 2010; Marriner et al., 2012b). Foraminifera, diatom and ostracod assemblages are dominated by brackish inner estuarine species such as *Cyprideis torosa*, *Leptocythere lagunae*, *Loxoconcha elliptica*, and *Cytherois fischeri*. The presence of opportunistic species tolerant of restricted conditions and ample food availability, such as *Hyanesina germanica*, *Ammonia perlucida* and *L. elliptica*, is consistent with a low-energy, organic-rich lagoonal basin without significant oxygen depletion on the lagoon bottom (Lachenal, 1989; Cimerman and Langer, 1991).

The evolution of a coastal lagoon from an open to semi-enclosed environment is commonly recorded in the buried lagoonal successions of the Mediterranean's clastic coastlines, in a so-called regressive sequence (e.g., Reineck and Singh, 1973; Caldara et al., 2008; Sabatier et al., 2010). The gradual development of sandy barriers favours the progressive isolation of the brackish water body with consequent silting and evaporation (Kjerfve, 1994). This leads to significant shallowing and silting of the semi-enclosed lagoons with respect to the open lagoons. The depth of these lagoons seldom exceeds a few decimetres (e.g., Ruiz et al., 2006; Vött, 2007) and the concomitant presence of macrophytes such as of *Ruppia maritima* and *Lamprothamnium papulosum* is consistent with maximum lagoon depths of −1 m (e.g., Primavera et al., 2011). Thus, samples found in inner or semi-enclosed lagoon facies (usually lagoonal shells, plant remains, organic sediments, wood or charcoal) have an associated indicative range from 0 to −1 m (Fig. 3B, Table 1).

We listed as undifferentiated brackish facies (Fig. 3B, Table 1) those samples that did not provide enough data to define a clear depositional environment (e.g., Correggiari et al., 1996) or that showed the presence of marsh plant macrofossils together with micro- and macro-fossil assemblages ranging from freshwater/slightly brackish taxa to shallow marine taxa (e.g., Colombaroli et al., 2007; Amorosi et al., 2013). For these samples, we assumed an indicative range from HAT to Mean

Lower Water MLW in order to encompass the whole tidal zone (Fig. 3B, Table 1). We added a further 0.5 m of additional error to account for the environmental uncertainty.

3.1.3. Beachrock index points

Beachrocks are a lithified coastal deposit where lithification is a function of CO_3^{-2} ion concentration in seawater, microbial activity and degassing of CO_2 from seaward flowing groundwater (Mauz et al., 2015b). Field experiments and coastal observations (e.g., Hanor, 1978; Hopley, 1986; Neumeier, 1998) suggest that cementation occurs within a few decades, in areas where suitable coastal morphology provides sufficient accommodation space for soft sediment to settle (Mauz et al., 2015b). The cement by which the loose sand and gravel are locked into position is indicative of the nearshore zone between the shoreface and the beach, at the interface between seawater and meteoric water (e.g., Neumeier, 1998; Vousdoukas et al., 2007). Issues on the use of beachrocks as accurate sea-level indicators are present in the literature (e.g., Kelletat, 2006). However, recent studies have demonstrated that the cement is crucial for identifying the spatial relationship between the coastline and the zone of beachrock formation (e.g., Vousdoukas et al., 2007; Mauz et al., 2015b).

Thus, a definition of the indicative meaning depends largely on the preservation of the original cement and its link with other sedimentary information (e.g., Mauz et al., 2015b). In the Mediterranean region, beachrocks have been sampled and dated down to −45 m (e.g., De Muro and Orrù, 1998; Orrù et al., 2004). Many studies have determined the vertical accuracy of beachrock samples through SEM, petrographic and cathodoluminescence analyses of cements with a precision up to ±0.25 m in microtidal settings (e.g., Desruelles et al., 2009; Vacchi et al., 2012b). Such vertical accuracy cannot be obtained without accurate description of the chemistry, crystal form and fabric of the cement. In the intertidal zone, the metastable aragonite and High Magnesium Calcite (HMC) form as irregularly distributed needles, isopachous fibres or rims and micritic cement (Neumeier, 1998; Desruelles et al., 2009). Samples having these characteristics have an indicative range spanning HAT to MLW (Fig. 3C, Table 1). However, 11 beachrock samples in our database did not meet these requirements because the original source did not contain enough information.

The beachrock formation zone (i.e. the mixing zone, Vousdoukas et al., 2007) can exceed the intertidal zone ranging from slightly subtidal to supratidal (spray zone). The amplitude of this zone depends on wave exposure and the local geomorphological setting and is not symmetrical with respect to the MSL because it is greater in the supratidal zone (Mauz et al., 2015b). For these samples, we thus adopted a conservative indicative range of +2 m MSL to −1 m MSL (Fig. 3C, Table 1). In our opinion, such approximation largely encompasses the mixing zone amplitude for the microtidal coasts of the Mediterranean.

3.2. Sea-level limiting points

Terrestrial limiting points usually form at an elevation above HAT, but can form in the intertidal zone due to rising groundwater tables (e.g., Engelhart and Horton, 2012). Therefore, a conservative lower limit of MSL has been employed in this analysis. In this database, terrestrial limiting points are typically samples deposited in freshwater marshes and swamps, alluvial plains, archaeological soils and on the subaerial part of beaches (Table 1).

Marine limiting points are typically samples deposited in open marine or prodelta environments as well as lagoonal environments that do not meet the requirements to be classified as index points. Further, in situ marine benthos (e.g. *Lithophaga* sp, *Mesophyllum* sp.) living in the infralittoral zone and with no direct relationship to a former midlittoral zone was converted into marine limiting point (Table 1).

Reconstructed RSL points must fall below terrestrial limiting points and above marine limiting points (example in Fig. 3B).

3.3. Archeological index and limiting points

The long history of human occupation in the western Mediterranean has left rich archaeological evidence along its coastlines, including, for instance, harbours, fish tanks, slipways and coastal quarries. Auriemma and Solinas (2009) furnished a synthesis of archaeological sea-level proxies. Many different archaeological structures that were originally emerged, or in contact with seawater, today lie below MSL and therefore attest to a relative change in the position of the sea surface and the structure. The "functional height" of an archaeological sea-level indicator corresponds to the elevation of a specific architectural part with respect to the MSL position at the time of its construction (e.g., Antonioli et al., 2007). Ancient port interface structures (e.g., quays and jetties), fishtanks and fishponds represent the most reliable sea-level indicators (e.g., Marriner and Morhange, 2007; Auriemma and Solinas, 2009; Morhange and Marriner, 2015) and have been used to produce index points in our database. In Section 2.2, we described the differences in the interpretations of fishtanks and fishponds as sea-level index points. There is considerable morphological variability in these structures (Higginbotham, 1997) and the definition of a standardized indicative meaning for the western Mediterranean scale is particularly challenging. For this reason, in our database the indicative meaning assigned to a fishtank index point encompasses the different archaeological interpretations (maximum two, see Section 2.2) provided by the original papers.

A variety of coastal archaeological structures, such as coastal quarries, tombs, breakwaters and coastal roads can provide insights to reconstruct the RSL in a given area (Auriemma and Solinas, 2009). However, due to the difficulties in establishing a relationship with a former MSL, we used these archaeological markers as terrestrial limiting points. Submerged structures, including harbour foundations and wrecks as well as the fine-grained sediments deposited inside the ancient ports (e.g., Marriner and Morhange, 2007), were used to produce marine limiting points.

3.4. Altitude of former sea-level

For each dated index point, RSL is estimated using the following equation:

$$RSL_i = A_i - RWL_i \quad (1)$$

(Shennan and Horton, 2002), where A_i is the altitude and RWL_i is the reference water level of sample i, both expressed relative to the same datum; MSL in our analysis.

The total vertical error is obtained by adding in quadratic individual errors according to:

$$e_i = \left(e^2{}_1 + e^2{}_2 + e^2{}_3 + e^2{}_n \ldots\right)^{1/2} \quad (2)$$

(Shennan and Horton, 2002), where $e_1, \ldots e_n$ represent the sources of error for each index point i including the indicative range (Fig. 3). The additional errors comprise an error associated with calculating the sample altitude. This can be as small as ±0.05 m with high precision surveying (e.g., Shennan, 1986), but can increase to more than ±0.5 m when the altitude was estimated using the environment in which the sample was collected (e.g., saltmarsh; Engelhart and Horton, 2012) or when the depths of the samples are measured with diving gauges (e.g., Rovere et al., 2010; Vacchi et al., 2012a). In southern France and Corsica, many data are expressed in relation to the local National Geodetic Datum (NGD) that is presently 0.1 m below MSL (e.g. Vella and Provansal, 2000; Morhange et al., 2013). All the data levelled to the NGD were therefore corrected.

A tidal error was included if the tidal information was based on multiple tidal stations or on tidal modeling. In our database this error does not exceed ±0.3 m, due to the microtidal setting of the Mediterranean. We included a core stretching/shortening sampling error ranging from

±0.15 m for rotary corers and vibracorers to ±0.05 m for hand coring (Hijma et al., 2015). The sample thickness is also incorporated into the sampling error term. For older bulk sediment samples, this may be as large as 0.25 m (e.g., Engelhart et al., 2015). We also calculated the angle of borehole error as a function of the overburden of the sample, taken in this study to be 1% (Tornqvist et al., 2008). We also included an environmental error that can be as up to 0.5 m in saltmarsh and lagoonal sediments not showing a clear depositional environment (see Section 3.1.2). The vertical error of the archaeological index points is not constant and is strongly related to the archaeological interpretations provided in the original papers. However, preservation of fossil biological zones on the archaeological structures may provide vertical uncertainties of up to 0.05 m (Marriner and Morhange, 2015).

Because of the lack of specific Mediterranean studies, we decided to not include an error term for potential changes in the paleotidal range (e.g., Hill et al., 2011). Nonetheless, it cannot be excluded that this error may have affected the indicative range of the data points during the Holocene.

To account for sediment compaction (e.g., Edwards, 2006), we subdivided the saltmarsh and lagoonal index points into basal and intercalated categories (Horton and Shennan, 2009). Basal samples are those recovered from within the sedimentary unit that overlies the incompressible substrate, but not directly at the intersection between the two (e.g., Engelhart and Horton, 2012). Basal samples may have undergone some consolidation since deposition. Intercalated samples correspond to organic horizons in between clastic layers and, therefore, they are generally most prone to compaction (e.g., Hijma et al., 2015). Where stratigraphic information was unavailable for an index point, we conservatively interpreted it as intercalated. Index points from archaeological markers, fixed biological and beachrock samples are virtually compaction free.

3.5. Age of sea-level indicators

In our database, the age of the samples was estimated using radiocarbon (^{14}C) dating of organic material from salt and fresh water marshes, marine and lagoonal shells, beachrock bulk cement as well as from the archaeological age of coastal structures. Because the production of atmospheric radiocarbon has varied through geological time, radiocarbon ages were calibrated into sidereal years with a 2σ range. All samples were calibrated using CALIB 7.0. We employed the IntCal13 and Marine13 (Reimer et al., 2013) datasets for terrestrial samples and marine samples, respectively. Where available, information on the necessary reservoir correction was taken either from the Marine Reservoir Database (Reimer and Reimer, 2001) or from published values. All index points are presented as calibrated years before present (ka BP), where year 0 is AD 1950 (Stuiver and Polach, 1977). A concern with old radiocarbon ages is the correction for isotopic fractionation (Tornqvist et al., 2015). This became a standard procedure at most laboratories by the late 1970s (Stuiver and Polach, 1977), but some laboratories have only applied this correction since the mid-1980s (Hijma et al., 2015).

In the database, the majority of ages were analyzed after 1990 and, therefore, most are not subject to this potential error. For the 31 ages that are affected, we followed the procedure of Hijma et al. (2015) to correct for isotopic fractionation. The age of the archaeological RSL data-points is given both by the period of construction and/or by the ^{14}C dating of biological indicators fixed on the coastal structures (Morhange and Marriner, 2015). In our database, the age of the archaeological RSL data-points is restricted to the last 5.0 ka BP.

3.6. Example of the production of a lagoonal index point from Malta

In order to better explain our new methodology for the production of index points in the Mediterranean, we here provide an example from a marsh coring in Malta. The sedimentary sequence from the coastal plain of Burmarrad is presented in Fig. 4 (Marriner et al., 2012b). The core BM1 (35.93 N°; 14.41° E) was obtained using a percussion corer (±0.15 m of sampling error) and has a surface elevation of +2 m MSL obtained using a high accuracy GPS (±0.05 m of levelling error) and extends to −15 m MSL. The base of the core (−15 m to −11 m) is composed of a dark grey unit dominated by silts and clay (47–98%). A charcoal (±0.05 m of thickness error) was sampled 12.1 m below the surface (0.12 m of angle error) and −10.1 below MSL. Radiocarbon dating of the charcoal yielded 6500 ± 30 ^{14}C years. The mollusc faunal density is low and dominated by lagoonal taxa (*C. glaucum*, *A. segmentum*) and the upper muddy-sand assemblage in sheltered areas (*Cerithium vulgatum*). The ostracods are dominated by brackish water (*C. torosa*) and freshwater (*Candona* cf. *lactea*, *Candona* cf. *compressa*, *Potamocypris variegata*, *Darwinula stevesoni*, *Illyocypris gibba*) species. The lagoonal taxa and low faunal densities indicate that the charcoal was deposited in an inner or semi-enclosed lagoon. Thus we assigned the charcoal sample a reference water at the midpoint between 0 and −1 m MSL (−0.5 m MSL) and an indicative range of 0 to −1 (±0.5 m). We are aware that charcoal found in lagoons may have been transported and yield ages older than the lagoon. Nonetheless, this error is inferior to the error margins associated with radiocarbon dating. In this instance, multiple samples (charcoal and peats) yielded coherent ^{14}C ages for this unit (Marriner et al., 2012b) supporting the chronology for this lagoonal environment.

The calculation of RSL and age, including the error terms, for this index point was:

$$\begin{aligned}\text{RSL} &= \text{-10.1 m} - (\text{-0.5 m}) \\ &= \text{-9.6 m} \\ \text{Error} &= \sum (0.5\ \text{m}^2{}_{\text{indicative range}} + 0.05\ \text{m}^2{}_{\text{levelling error}} \\ &\quad + 0.2\ \text{m}^2{}_{\text{sampling and thikness errors}} + 0.12\ \text{m}^2{}_{\text{angle error}})^{1/2} = 0.55\ \text{m}\end{aligned}$$

$$\text{Age} = 6500 \pm 30\,{}^{14}\text{C years} = (7326\ \text{ka}\ 7471\ \text{ka BP}\ 2\sigma).$$

4. Predictions of RSL

The RSL model predictions presented in the following sections have been obtained by solving the Sea-level Equation (SLE, Farrell and Clark, 1976). The SLE, which describes the spatiotemporal variations of sea-level associated with the melting of late Pleistocene ice sheets, has been solved numerically by means of an improved version of the open source code SELEN (Spada and Stocchi, 2007). SELEN assumes a laterally homogeneous, spherical, incompressible and self-gravitating Earth with Maxwell rheology. It includes the effects of rotational fluctuations on sea-level (Milne and Mitrovica, 1998) and accounts for horizontal migration of shorelines following the method outlined by Peltier (2004). In all our computations, we have employed the ICE-5G model of Peltier (2004) to predict a nominal RSL curve, based on a three-layer approximation of the multi-layered viscosity profile VM2 (Table 2). To account for the uncertainties in the viscosity profiles, we performed further runs varying the viscosity profiles in each layer within a reasonable range; the minimum and maximum viscosity values are shown in Table 2. The thickness of the elastic lithosphere has been kept constant (90 km) in all of our calculations.

5. Results

We re-assessed 917 radiocarbon and archeologically dated RSL data-points along the western Mediterranean Sea. We reconstructed the RSL histories of 22 regions using a database composed of 469 index points and 177 limiting points (Appendix A, references of the original sources in Appendix B, Fig. 5A,B). We excluded 271 sea-level datapoints (113 index points and 158 limiting points), which were deemed to not be appropriate for the RSL reconstructions (Appendix C). For instance, we discarded the RSL data-points that may have been significantly affected by local co-seismic tectonic uplift or subsidence. For example, near Punta delle Pietre Nere (North Apulia region, #21), Mastronuzzi

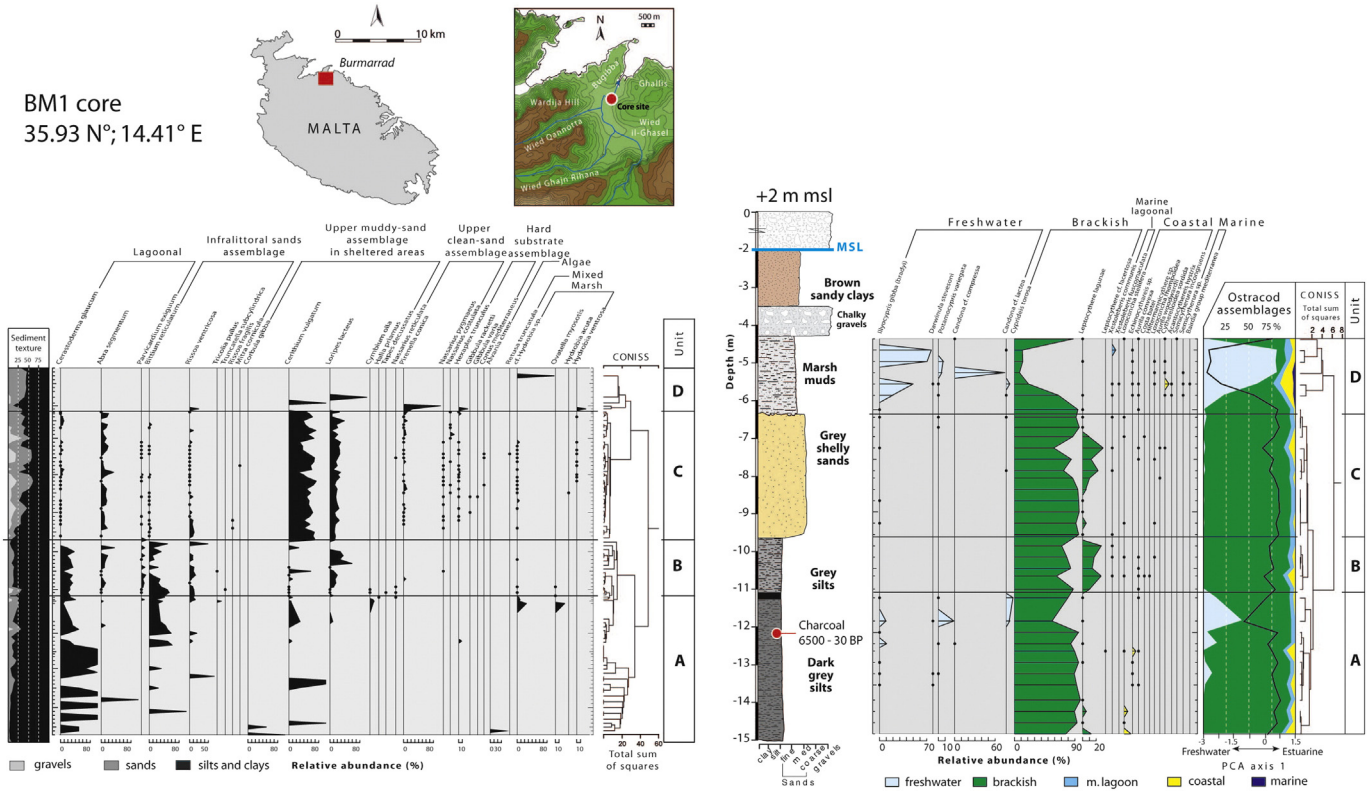

Fig. 4. Location of the example site in Burmarrad, Malta. Molluscan and ostracod assemblages of the core BM1 indicate that the dated charcoal was deposited in semi-enclosed lagoon facies. The sample, collected at −10.1 MSL yielded a radiocarbon age of 6500 ± 30 years (7326–7471 ka BP 2σ). After correction for the indicative range, we produced an index point placing the RSL at −9.6 ± 0.55 (details in Section 3.3).

and Sanso (2002); Mastronuzzi and Sansò (2012) provided evidence for a co-seismic RSL change greater than 0.5 m at ~1624 AD. Similarly, on Pag Island (Nortwestern Adriatic #17), detailed investigation indicated a co-seismic subsidence at ~1100 AD (Marriner et al., 2014). Therefore, at sites where co-seismic vertical movements were documented by previous studies, we did not use the RSL data-points older than the seismic event, whose current position was significantly influenced by the rapid vertical movement. Obviously, we cannot exclude that presently unknown seismic events may have influenced the position of some index points in tectonically active regions included in our database.

We further excluded the RSL data-points showing a high degree of compaction. For instance, an index point placing the RSL at ~−11.1 m MSL at ~6.7 ka BP in the Rhone Delta (Southern France, #3, Vella et al., 2005, Appendix C) is inconsistent with a suite of points placing the RSL at least ~5 m higher at the same time. This evaluation was only possible at sites where RSL reconstruction was based on multiple proxies. Reconstructions based on small datasets or only on intercalated samples are thus less reliable and caution must be used when comparing these data with the GIA models.

In addition, we rejected a large amount of data not useful for RSL reconstruction. For example, a marine limiting point constraining the RSL above ~−14.2 m MSL at ~5.2 BP in Northern Corsica and Pianosa (#6, Sartoretto et al., 1996, Appendix C) is not useful because several other data-points demonstrate that RSL was already above ~−6 m MSL at this time (Fig. 7, #6). Finally, we excluded samples with poor or absent descriptions of the depositional environments.

Spatially, RSL reconstructions covered most of the northwestern Mediterranean coast whereas Tunisia represents the sole region located on the southern Mediterranean seaboard, where data paucity did not allow a robust RSL reconstruction for Algeria and Morocco (Fig. 1). The age range of the data spans the last 14 ka, with constant increase in the number of index and limiting points throughout the Holocene (Fig. 5B). Compaction-free index points (e.g., *L. byssoides*, beachrocks and archeological index points) and basal index points represent 28% and 14% of the database, respectively. The majority (52%) of the index points included in the database is intercalated (Fig. 5B).

Table 2
Viscosity parameters used to predict the nominal, maximal and minimal RSL curve for each region.

ICE 5G VM2	Viscosity parameters (Pa s)		
	Upper mantle	Transition zone	Lower mantle
Nominal	$0.5\ 10^{21}$	$0.5\ 10^{21}$	$2.7\ 10^{21}$
Maximal	$0.8\ 10^{21}$	$0.8\ 10^{21}$	$5.0\ 10^{21}$
Minimal	$0.2\ 10^{21}$	$0.2\ 10^{21}$	$1.0\ 10^{21}$

5.1. Central Spain (#1)

The RSL history of the Central Spanish coast is composed of 13 index points and 13 limiting points (Fig. 6, #1) from coastal areas between Valencia and Alicante. The oldest index point places the RSL at −16.0 ± 0.6 m at ~9.1 ka BP. RSL rose to −10.6 ± 0.6 m at ~8.6 ka BP and to −6.1 ± 0,7 m at ~8.3 ka BP. Two points document the progressive rise between ~8.3 and ~7.1 ka BP when an index point places the RSL at −3.5 ± 0.5 m. Two marine limiting points (shallow shoreface) indicate RSL was slightly above −2 m at ~6.5 ka BP. Between ~6.0 and ~5.0 ka BP terrestrial samples constrain the RSL below the present datum. Late Holocene intercalated index points show scatter, most likely related to sediment compaction. Less compacted index points indicate that RSL was at −0.9 ± 0.6 m at ~3.4 ka BP and at −0.3 ± 0.5 m at 1.1 ka BP.

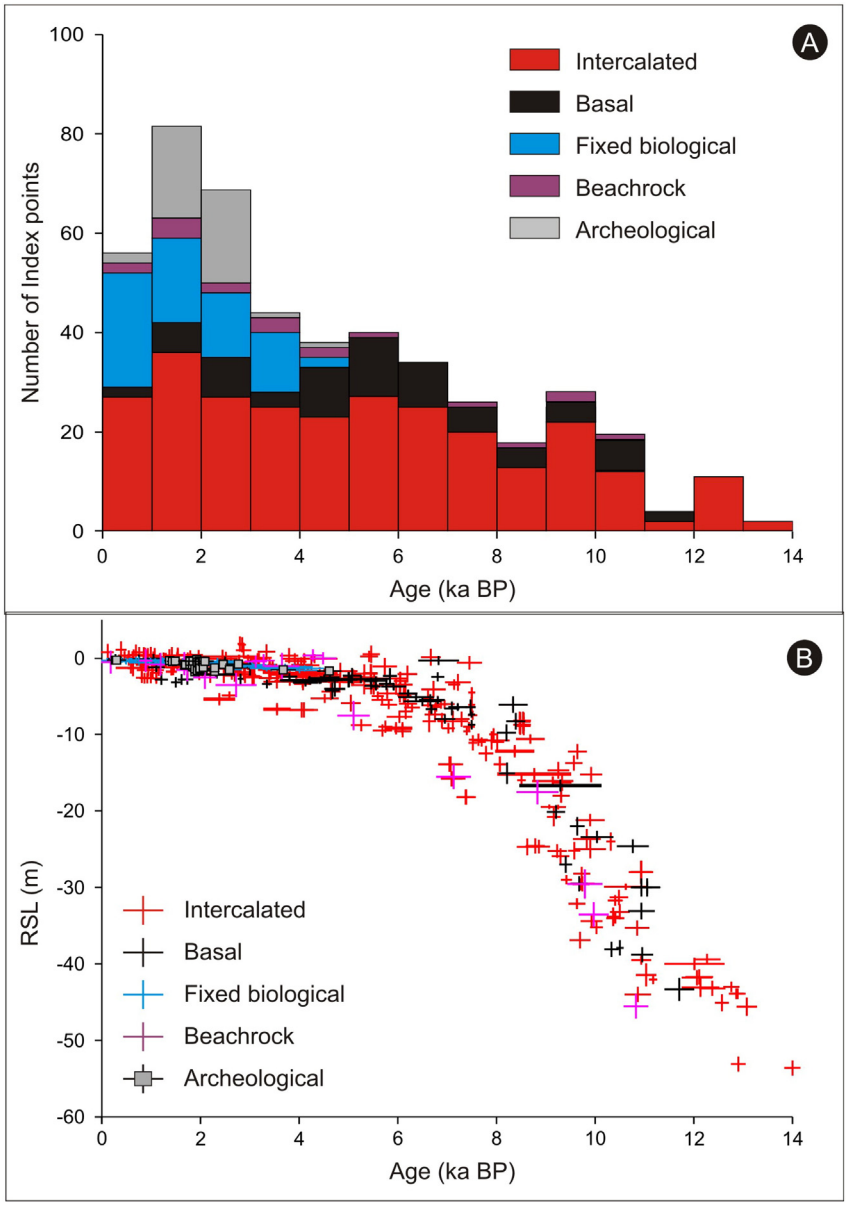

Fig. 5. A) Stacked histogram of intercalated, basal, fixed biological, beachrocks and archaeological index points. B) Total plots of the 469 index points used for the RSL reconstructions in the 22 regions. Index points are divided into intercalated, basal, fixed biological, beachrocks and archeological indicators.

5.2. Northern Spain (#2)

The Northern Spanish coast database is composed of 19 index points and 6 limiting points (Fig. 6, #2). Index points and limiting dates derive from cores on the Ebro and Llobregat deltas and Cubelles coastal plain, in addition to beachrocks and *L. byssoides* samples collected in Costa Brava. Archeological investigations near Empuriès provided marine limiting samples. At ~12 ka BP, RSL was at −40 ± 0.9 m. Younger index points document that RSL rose rapidly to −12.1 ± 0.7 m at ~8.3 ka BP. The suite of mid-Holocene index points from Cubelles coastal plain indicates RSL was at −3.4 ± 0.8 m at ~5.7 ka BP and at −1.2 ± 1.2 m at ~4.0 ka BP. Intercalated index points from the Ebro Delta show evidence of compaction, most likely due to the weight of the overlying sediment body. In fact, at ~5.9 ka BP, one index point from the Ebro Delta places the RSL at −9.1 ± 0.7 m and at ~3.6 ka BP at −6.6 ± 0.7 m. One *L. byssoides* index point indicates RSL was already at −0.4 ± 0.5 m at ~2.3 ka BP. Thereafter, RSL remained within −0.7 m of present day.

5.3. Central France (#3)

The RSL history of central France is based on 80 index points and 16 limiting points (Fig. 6, #3). Data derive from marsh and lagoon cores on the Rhone Delta, Berre lagoon and the Languedoc coastal area. Samples comprise *L. byssoides* collected at Port Cros National Park and La Ciotat, as well as fixed fauna from archeological excavations in Marseille. One basal index point places the RSL at −43.3 ± 1.5 m at ~11.7 ka BP. Index and limiting points constrain a rapid sea-level rise to the early Holocene. At ~10.6 and at 7.5 ka BP, RSL was at −29.9 ± 0.4 m and at −7.4 ± 0.4 m, respectively. The rate of RSL declined in the mid-Holocene. At 5.0 ka BP, multiple basal index points indicate RSL was ~−2.8 m. Index points for the last 4.6 ka BP show significant scatter. Basal peat samples from the Rhone Delta indicate a sea-level stillstand at ~−2.5 m between ~4.6 and ~3.5 ka BP. Conversely, in the same period, both archaeological index points and *L. byssoides* index points indicate a

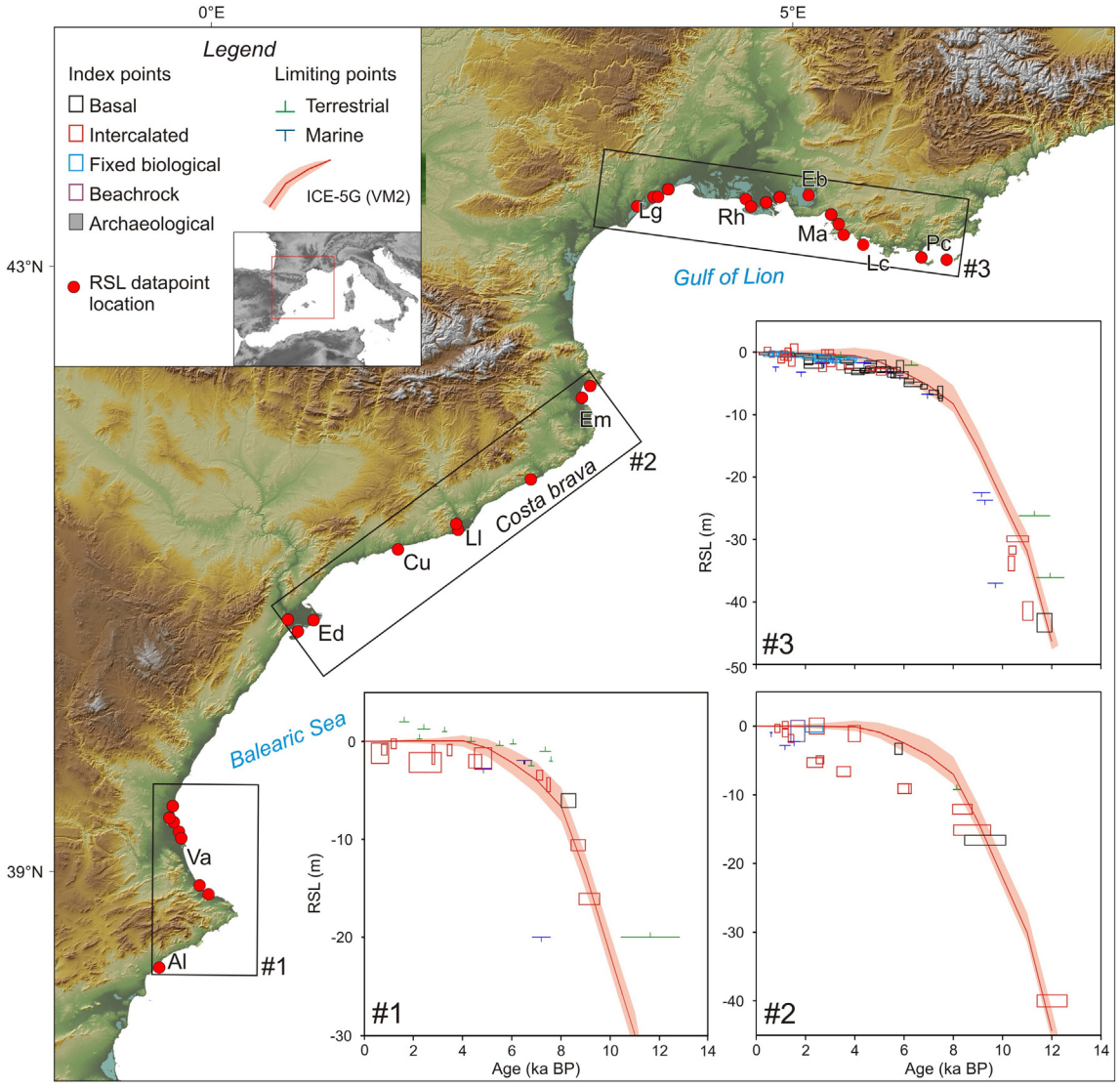

Fig. 6. RSL reconstructions in central Spain (#1), northern Spain (#2) and central France (#3). Index points (boxes) are plotted as calibrated age against change in sea level relative to present. Limiting points are plotted as terrestrial or marine horizontal lines. Dimensions of boxes and lines for each point based on 2s elevation and age errors. The relative sea-level data is compared to a prediction (red line with minimum and maximum errors) from the SELEN model (see Section 4). Al, Alicante; Va, Valencia. Ed, Ebro Delta; Cu, Cubelles; Ll, Llobregat Delta; Em, Empuries. Lg, Languedoc lagoons; Rh, Rhone Delta, Eb, Etang de Berre, Ma, Marseille; Lc, La Ciotat; Pc, Port Cros.

continuous rise in sea-level with multiple index points that constrain the RSL to ~−1.5 m at ~3.5 ka BP. Rising rates decreased during the remaining part of the Holocene. Multiple archaeological and *L. byssoides* index points indicate RSL was at ~−0.8 m at ~2.5 ka BP, rising to ~−0.8 m at ~1.5 ka BP. During the last 1.0 ka BP, RSL remained within 0.3 m of modern MSL.

5.4. Western Ligurian Sea (#4)

The RSL database of the western Ligurian Sea consists of 19 index points and 18 limiting dates (Fig. 7, #4). Archeological excavations in the ancient harbours near Frejus and Genova provided index and limiting points. Additional data derived from cores performed on the coastal plains near Nice (France), Savona and Genova (Italy). Index points also derived from *L. byssoides* samples collected near Frejus and Nice, and from a beachrock sample collected near Savona (Italy). At ~13.0 ka, index and limiting points constrain the RSL to −45.6 ± 1.2 m. Then, RSL rose rapidly to −18 ± 0.9 m at ~9.3 ka BP. During the mid-Holocene (from ~7.5 to ~5.7 ka BP), RSL was between −6.1 ± 1 m and −1.1 ± 1.1 m. Index points in the Late Holocene show scatter. Archeological and *L. byssoides* index points suggest a continuous rise of RSL, from −0.9 ± 0.4 m at ~3.0 ka BP to −0.4 ± 0.3 at ~2.0 ka BP, followed by a gradual rise to the present datum.

5.5. Eastern Ligurian Sea (#5)

The RSL history of the northeastern Ligurian Sea is based on 21 index points and 9 limiting points from cores on the Versilia plain and the Arno river coastal plain (Fig. 7, #5). Additional data-points derive from archaeological investigations near Pisa and La Spezia. RSL was at −45.1 ± 1.1 m at ~12.5 ka BP. Then, basal index points indicate that RSL rose rapidly to −13.9 ± 1.0 m at ~8.0 ka BP and to −6.7 ± 0.6 m at ~6.6 ka BP. RSL rise slowed down in the remaining part of the Holocene. At ~4.2 ka BP, multiple intercalated index points place the RSL at ~−2.2 m. Late Holocene RSL is loosely constrained by the data. The youngest intercalated index point places the RSL at −1 ± 0.6 m at ~2.2 ka BP. Younger terrestrial limiting points constrain the RSL above −0.2 m at ~2.0 ka BP.

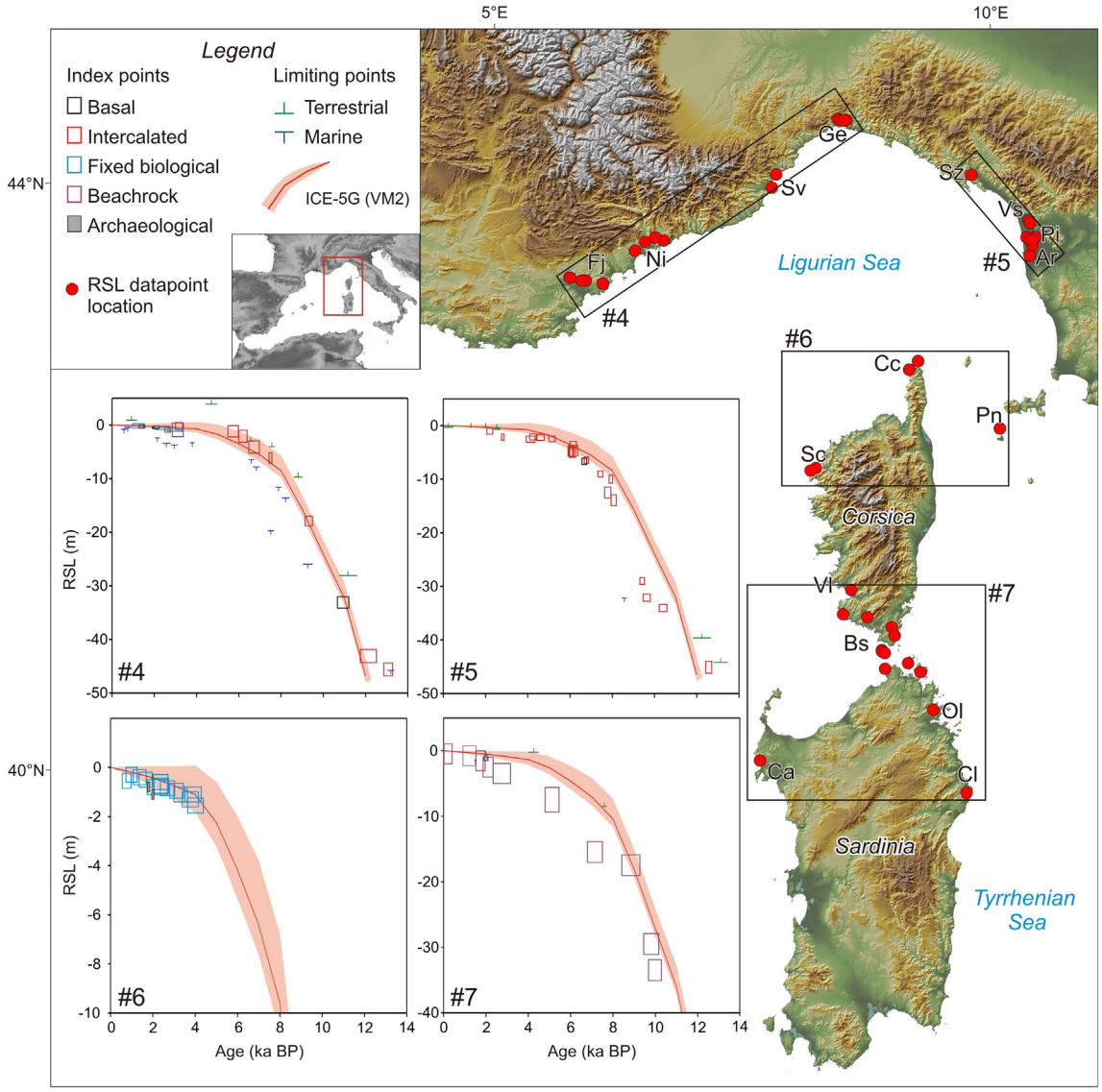

Fig. 7. RSL reconstructions in western Ligurian Sea (#4), eastern Ligurian Sea (#5), northern Corsica and Pianosa (#6) and southern Corsica and northern Sardinia (#7). Index points (boxes) are plotted as calibrated age against change in sea level relative to present. Limiting points are plotted as terrestrial or marine horizontal lines. The dimensions of boxes and lines for each point are based on 2s elevation and age errors. The relative sea-level data is compared to a prediction (red line with minimum and maximum errors) from the SELEN model (see Section 4). Red dots denote the approximate location of the cluster of RSL data-points. Fj, Frejus; Ni, Nice coastal plain; Sv, Savona; Ge, Genova. Sp, La Spezia; Vs, Versilia coastal plain, Pi, Pisa; Ar, Arno coastal plain. Cc, Cap Corse; Sc, Scandola; Pn, Pianosa. Vl, Gulf of Valinco; Bs, Bonifacio Strait; Ol, Olbia; Cl, Cala Liberotto, Ca, Capo Caccia.

5.6. Northern Corsica and Pianosa (#6)

The RSL history for this region is restricted to the late Holocene and is presented in Fig. 7 (#6). The database is composed of 15 index points from *L. byssoides* samples collected in Scandola, and Cap Corse in northern Corsica. Additional index and limiting points derive from archaeological surveys carried out on Pianosa Island (Italy). The oldest index point places the RSL at -1.5 ± 0.4 m at ~4.0 ka BP. Younger index points show a continuous sea-level rise. RSL was at -0.8 ± 0.4 m at ~2.0 ka BP, at -0.5 ± 0.4 m at ~1.6 ka BP and at -0.3 ± 0.4 m at ~1.0 ka BP. Archeological index points place the RSL at -1.1 ± 0.2 m at ~2.0 ka BP and at -0.8 ± 0.2 m at ~1.0 ka BP.

5.7. Southern Corsica and northern Sardinia (#7)

The database for southern Corsica and northern Sardinia consists of 11 index points from beachrock samples collected in the Bonifacio strait and in northeastern Sardinia (Fig. 7, #7). Additional limiting points were obtained from cores in Gulf of Valinco (Corsica) and from archeological surveys in Bonifacio Strait, Capo Caccia, and Olbia (Sardinia). During the early Holocene, RSL rose from -33.5 ± 1.6 m at ~10.0 ka BP to -17.5 ± 1.6 m at ~8.3 ka BP. RSL is loosely constrained between ~8.0 and ~2.5 ka BP. Younger index and limiting points indicate RSL was between ~−0.7 and ~−1.5 m between ~2.0 and ~2.0 ka BP. At ~0.8 ka BP, one beachrock index point places the RSL at -0.8 ± 1.5 m.

5.8. Southwestern Sardinia (#8)

The RSL history of southern Sardinia comprises 18 index points and 8 limiting points (Fig. 8, #8). Data were obtained from cores in Cagliari, in the Gulf of Oristano, in Piscinni Bay and near archaeological sites in Tharros, Nora, Malfatano Cape and Sant'Antioco. The oldest index point at ~10.8 ka BP estimates that RSL was at -45.5 ± 1.6 m. RSL rose to -29.5 ± 1.0 m at ~9.7 ka BP and to -27 ± 1.0 m at ~9.4 ka BP. At ~7.0, RSL was at -13.9 ± 1 m MSL. Between ~4.6 and 4.0 ka BP, index points show considerable scatter. One intercalated sample from Cagliari places the RSL at -6.8 ± 1.0 m while one sample from

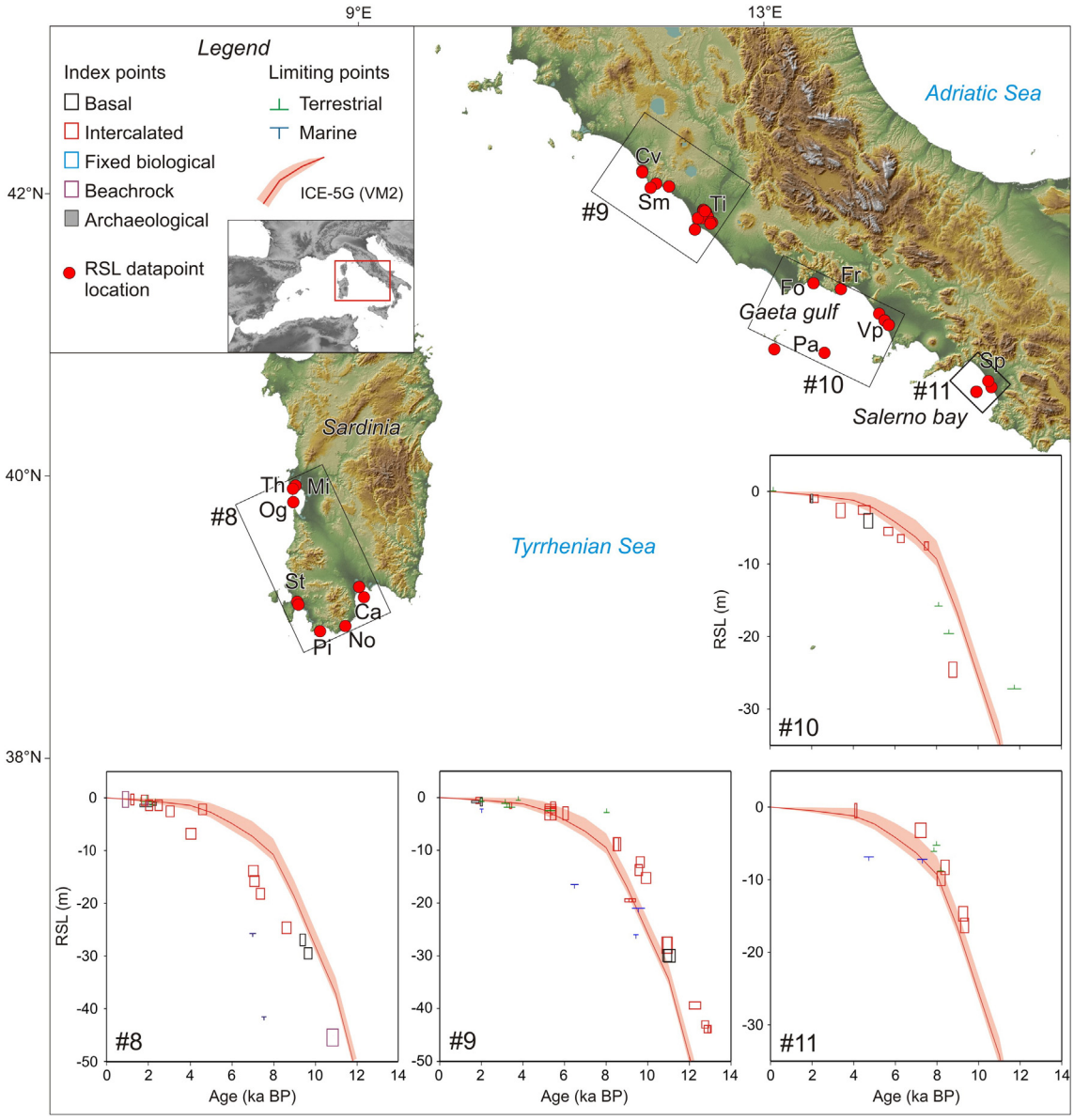

Fig. 8. RSL reconstructions in southwestern Sardinia (#8), north-central Latium (#9), Gulf of Gaeta (#10) and Salerno Bay (#11). Index points (boxes) are plotted as calibrated age against change in sea level relative to the present. Limiting points are plotted as terrestrial or marine horizontal lines. Dimensions of boxes and lines for each point based on 2s elevation and age errors. The relative sea-level data are compared to a prediction (red line with minimum and maximum errors) from the SELEN model (see Section 4). Red dots represent the approximate location of RSL data-points. Th, Tharros, Mi, Is Mistras, Or, Gulf of Oristano, Pi, Piscinni Bay and Malfatano Cape; St, Sant'Antioco; Ca, Cagliari; No, Nora. Cv, Civitavecchia; Sm, Santa Marinella, Ti, Tiber Delta. Fo, Fondi coastal plain; Fr, Formia; Po, Pontine Archipelago; Vp, Volturno coastal plain. Sp, Sele coastal plain.

Is Mistras places the RSL at −2.2 ± 1.0 m. Late Holocene index and limiting points indicate that RSL rose to within ~1.4 m of modern MSL from ~2.5 ka BP to present.

5.9. North-central Latium (#9)

The RSL history for the northern Latium coast spans the early Holocene to present and constitutes 36 index points and 13 limiting points (Fig. 8, #9). Data derive from salt and freshwater marshes from the Tiber Delta and from archaeological investigations carried out on the Tiber Delta (Portus and ancient Ostia), near Santa Marinella and Civitavecchia (Fig. 8, #9). The two oldest index points place the RSL at −43.9 ± 0.7 m at ~12.8 ka BP. A suite of intercalated and basal index points shows a rapid rise between ~12.7 and ~10.9 ka BP when RSL was at −28 ± 0.5 m. There is considerable scatter in the younger intercalated index points, probably reflecting the influence of water and organic content, long-term tectonic uplift and the depositional history of the Tiber Delta. At ~8.5 ka BP, multiple intercalated index points place the RSL at −8.9 ± 1.2 m and between −3.1 and −2.1 m at ~5.5 ka BP. The Late Holocene RSL history is poorly constrained.

At ~2.0 ka BP, different archaeological interpretations (see Section 2.2) of Roman fishtanks place the RSL between ~−1.3 m and ~−0.4. At ~2 ka BP, one intercalated index point places the RSL at −0.6 ± 0.6 m and a further archaeological index point indicates RSL was at −0.8 ± 0.2 m at ~1.7 ka BP.

5.10. Gulf of Gaeta (#10)

The database for the northern Campania coast consists of 11 index points and 5 limiting points from cores on the Volturno and Fondi plain and archaeological surveys in Formia and the Pontine archipelago (Fig. 8, #10). A terrestrial limiting point suggests RSL was below ~−27.0 m at ~11.7 ka BP. The oldest intercalated index point places the RSL at −24.6 ± 1.0 m at ~8.8 ka BP. RSL rose to −7.5 ± 0.6 m at

~7.5 ka BP. At ~4.7 ka BP, one basal index point places the RSL at −4.1 ± 1.0 m. During the Late Holocene, one intercalated index point indicates RSL was at −2.6 ± 1.0 m at ~3.3 ka BP and at −1.0 ± 0.5 m at ~2.1 ka BP. During the same period, different archaeological interpretations of Roman fish tanks place the RSL between ~−1.3 and ~−0.6 ± 0.2 m.

5.11. Salerno Bay (#11)

The RSL history of Salerno Bay consists of 6 index points and 5 limiting points and is restricted to the mid-Holocene (Fig. 8, #11). Data are all from cores taken on the coastal plain of Sele river. Further limiting points derive from offshore coring in Salerno Bay. At ~9.3 ka BP, RSL was at −16.3 ± 1.1 m. RSL rose to −8.3 ± 1.1 m at ~8.4 ka BP. From ~8 to ~7.2 ka BP, limiting points constrain the RSL between −5.3 and −7.2 m. A younger index point places the RSL at −0.5 ± 1.0 m at ~4.1 ka BP.

5.12. Northwestern Sicily (#12)

The RSL history of northwestern Sicily comprises 9 index points and 5 limiting points. Data come from a lagoon core near Marsala and from fossil vermetid reefs in Capo San Vito and near Palermo (Fig. 9, #12). Additional limiting points derive from fossil marine shells collected on Marettimo Island and near Palermo and archaeological investigations in the Punic town of Mozia. The oldest limiting points constrain the RSL below ~−27 m and above ~−25 m at ~9.5 ka BP. There is a hiatus of data up to ~2.8 ka BP when an index point places the RSL at −1.1 ± 0.6 m. RSL rose to −0.4 ± 0.6 m at ~2.5 BP and was within ~0.3 m during the last 1 ka BP.

5.13. Mid-eastern Sicily (#13)

The database for mid-eastern Sicily includes 14 index points and 7 limiting points. Data are from archaeological surveys near Syracuse and lagoon cores near Augusta, Catania and Syracuse (Fig. 9, #13). The oldest intercalated index point places RSL at −36.9 ± 1.1 m at ~9.6 ka BP. A limiting point constrains the RSL above ~−20 m at ~8.1 ka BP. RSL rose rapidly to −6.2 ± 1.0 m at ~6.6 ka BP and to −2.3 ± 1.0 m at ~4.2 ka BP. Late Holocene data-points show significant scatter, most likely related to the uplift trend affecting the area (see Section 2.1). Intercalated index points from Augusta and Priolo indicate that RSL reached the present datum at ~3.7 ka BP. Conversely, archaeological data-points indicate RSL was between −3 and −1.2 m at ~3.7 ka BP and at −1.5 m ± 0.3 m at ~2.6 ka BP.

5.14. Southern Sicily and Malta (#14)

The RSL history for Southern Sicily and Malta is restricted to the mid and late Holocene. The database is composed of 14 index points and 9 limiting points from lagoon cores near Pachino (Sicily) and in Burmarrad (Malta). Additional limiting points derive from archaeological surveys undertaken in Avola (Sicily) and along the Maltese coast near Marsaxlokk (Fig. 9, #14). The oldest intercalated index point places the RSL at −11.1 ± 1.0 m at ~7.5 ka BP. At ~6.1 ka BP, index and limiting points constrain the RSL to ~-7 m. Two index points indicate RSL was between −4.4 m and −3.2 m at ~4.7 ka. RSL slowed in the late Holocene.

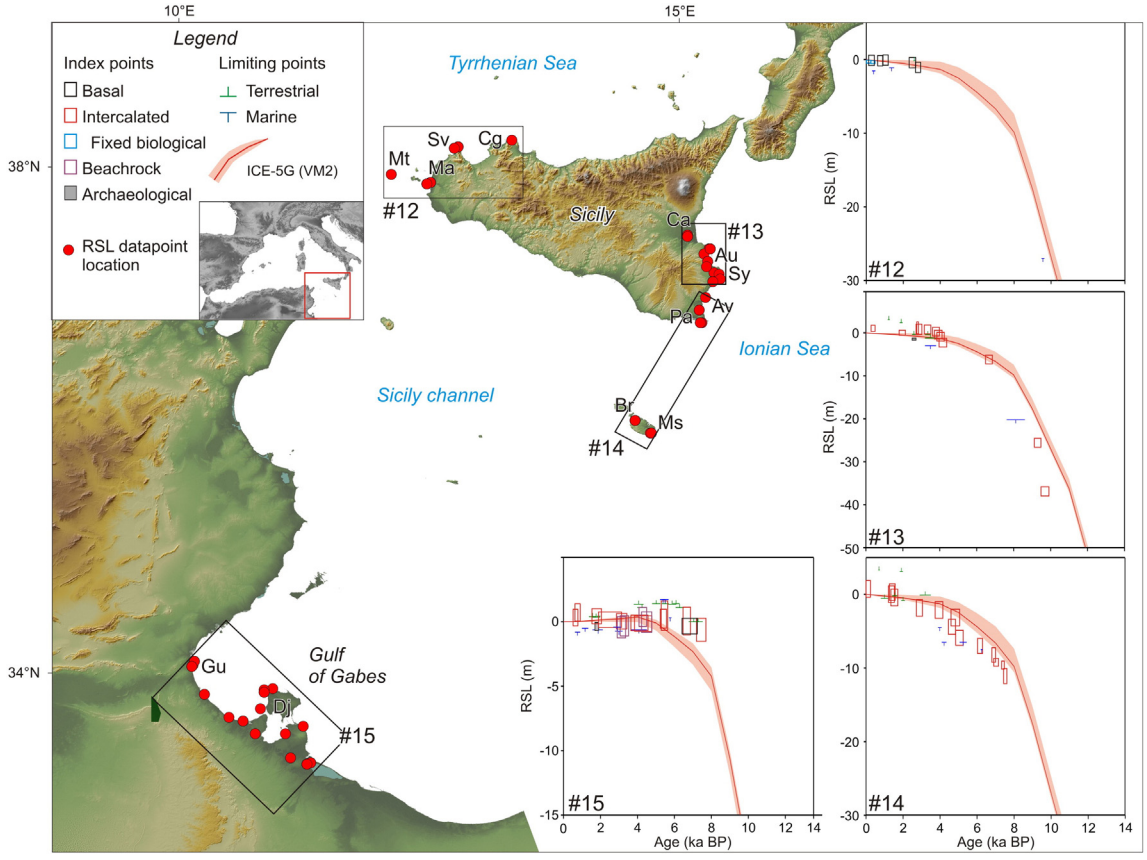

Fig. 9. RSL reconstructions in northwestern Sicily (#12), mid-eastern Sicily (#13), southeastern Sicily (#14) and southern Tunisia (#15). Index points (boxes) are plotted as calibrated age against change in sea level relative to present. Limiting points are plotted as terrestrial or marine horizontal lines. Dimensions of boxes and lines for each point based on 2s elevation and age errors. The relative sea level data is compared to a prediction (red line with minimum and maximum errors) from the SELEN model (see Section 4). Red dots denote the location of RSL data-points. Mt, Marettimo; Ma, Marsala sound; Sv, Cape San Vito; Pl, Palermo. Ca, Catania coastal plain; Au, Augusta; Sy, Syracuse. Av, Avola; Pa, Pachino; Br, Bourammad, Ms, Marsaxlokk. Dj, Djerba Island; Gu, Gulf of Gabes.

RSL was at −2.1 ± 1.1 m at ~3.9 ka BP and at −1.8 ± 1.1 m at 2.8 ka BP. A limiting point constrains the RSL below −0.8 m at ~2.0 ka BP. Multiple index and limiting points indicate RSL rose to within ~1 m of modern MSL from ~1.5 ka BP to present.

5.15. Southern Tunisia (#15)

The RSL database for the southern Tunisian coast includes 18 index points and 20 limiting points and is restricted to the last ~7.4 ka BP (Fig. 9, #15). Data come from a lagoon core in the Gulf of Gabes, as well as from beachrock samples and archaeological surveys undertaken near Djerba Island. RSL was −0.6 ± 0.9 m at ~7.4 ka BP and rose to 0.1 ± 1.1 m at ~6.8 ka BP. Multiple index limiting points indicate RSL was above the present MSL for the remaining part of the mid-Holocene. Two marine limiting points constrain it to above 1.7 ± 0.3 m at ~5.5 ka BP while terrestrial limiting points suggest RSL did not exceed 1.4 ± 0.4 m during the same period. At ~4.0 ka BP, RSL dropped to the present datum and remained within ~−0.4 m and ~0.4 m in the late Holocene. Intercalated index points indicate RSL was at 0 ± 0.6 m at ~3.1 ka BP and at 0.1 ± 0.6 m at ~2.5 ka BP. At ~1.8 ka BP, two archeological index points place the RSL at ~−0.3 m while an intercalated index point places the RSL at 0.4 ± 0.6 m. At ~0.6 ka BP, RSL was at −0.1 ± 0.6 m.

5.16. Venice and Friuli lagoons (#16)

The RSL history in this region is composed of 49 index points and 9 limiting points (Fig. 10, #16). Most of the data are from coring and geoarchaeological surveys of Venice lagoon. Additional index and limiting points derive from cores on the Friuli coastal plain and the lagoons of Grado-Marano and Caorle, and near the town of Monfalcone. RSL is not well constrained in the early Holocene with the oldest limiting point placing the RSL below −23.5 m at ~9.7 ka BP. A suite of basal index points documents a continuous rise in RSL during the mid-Holocene. RSL was at −9.3 ± 0.8 m at ~7.5 ka BP rising to −5.5 ± 0.8 m at ~6.6 ka BP. At ~5.5 ka BP, index and limiting points indicate RSL was at ~−3m. There is considerable scatter in the late-Holocene index points, most likely due to compaction. Multiple index points indicate RSL was between −1 and −2 m at ~4.0 ka BP. One basal index point indicates that RSL rose to −1.4 ± 0.7 m at ~2.5 ka BP. Scatter in the index points increases during the last ~2.0 ka and the large error bars did not allow us to satisfactorily reconcile the RSL history during this period. However, the youngest index point places the RSL at −0.4 ± 0.6 m at ~0.6 ka BP. A younger limiting point constrains the RSL to below −0.3 m at ~0.3 ka BP.

5.17. Northeastern Adriatic Sea (#17)

The RSL database for the northeastern Adriatic Sea is composed of 28 index points and 6 limiting points (Fig. 10, #17). Data come from marsh and lagoon cores near Trieste, on the Istrian coast and on Pag Island. Offshore cores undertaken during geological and geo-archaeological surveys in the Gulf of Trieste and on the Istrian coast provided additional index and limiting points. The oldest limiting point places the RSL below -28 m at 10.9 ka BP. During the early Holocene, multiple intercalated index and limiting points indicate that RSL was between −28 and −23 m between 10 and 9.6 ka BP. However, one basal index point places the RSL at −22 ± 1.2 m at ~9.6 ka BP. In the mid-Holocene, two basal index points constrain the RSL to -2.9 ± 1.0 m at ~5.0 ka BP. At ~3.1 ka BP one intercalated index point from Trieste placed the RSL at −0.1 ± 0.8 m while a coeval basal index point from the Istrian coast places the RSL at -1.29 ± 1.1 m. At ~2.0 ka BP multiple archaeological index and limiting points place the RSL between −1.75 and −1.4 m. In the northern part of the Gulf of Trieste, the archaeological data are

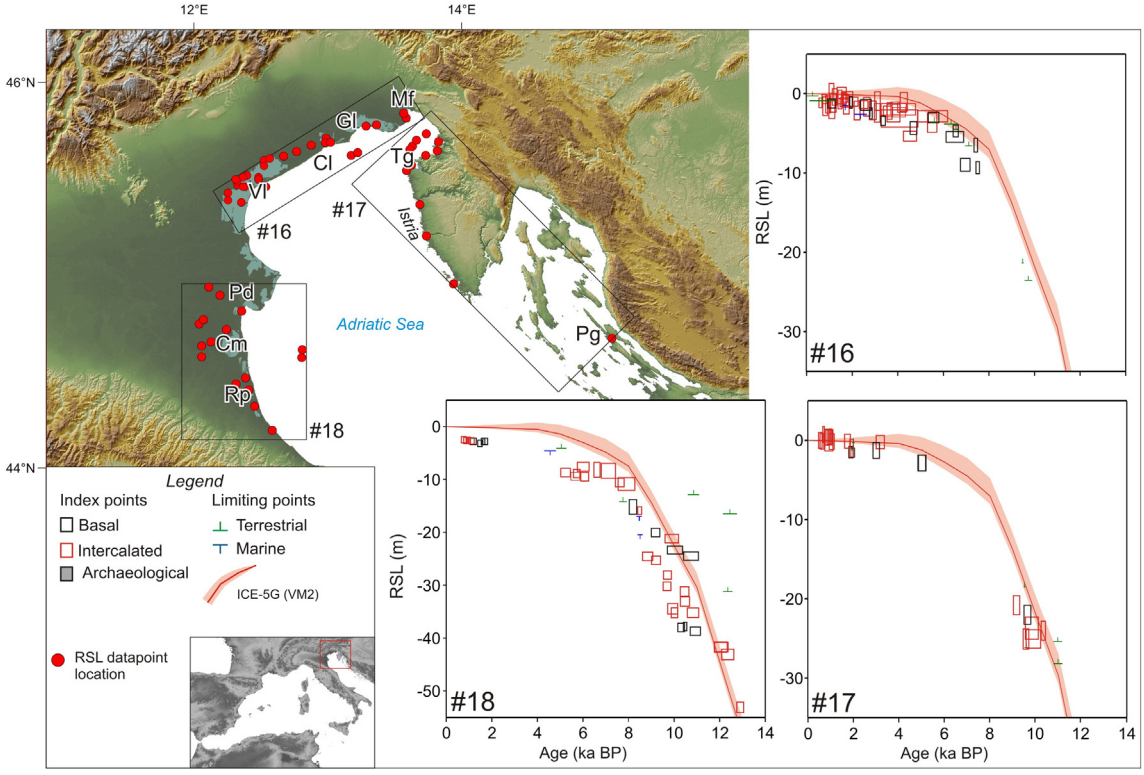

Fig. 10. RSL reconstructions in Venice and Friuli lagoons (#16), northeastern Adriatic Sea (#17), and northwestern Adriatic Sea (#18). Index points (boxes) are plotted as calibrated age against change in sea level relative to the present. Limiting points are plotted as terrestrial or marine horizontal lines. Dimensions of boxes and lines for each point based on 2s elevation and age errors. The relative sea-level data are compared to a prediction (red line with minimum and maximum errors) from the SELEN model (see Section 4). Red dots represent the approximate location of RSL data-points. Vl, Venice lagoon; Cl, Caorle lagoon; Gl, Grado lagoon; Mf, Monfalcone. Tr, Gulf of Trieste, Pg, Pag Island. Pd, Po Delta; Cm, Comacchio coastal plain; Rp, Romagna coastal plain.

in agreement with a lagoonal index point placing the RSL at −1.0 ± 1.1 m at ~1.9 ka BP. Younger records indicate RSL has been within ~-0.5 of modern MSL during the last ~1.5 ka BP.

5.18. Northwestern Adriatic Sea (#18)

The database for the northwestern Adriatic Sea is composed of 40 index points and 9 limiting points. Data derive from cores collected on the southern part of the Po Delta, near Comacchio and on the Romagna coastal plain (Fig. 10, #18).

RSL is well constrained in the early to mid Holocene. By contrast, few data are available for the late Holocene. The oldest index points place the RSL at −53.0 ± 0.9 m at ~12.9 ka BP. A suite of index points indicate that RSL rose to ~−43.0 m at ~12.2 ka BP. Younger data show scatter, most likely related to the variability in subsidence rates driven by the sediment compaction. However, a suite of basal index points indicates a rapid rise in RSL in the remaining part of the early Holocene. RSL was at -23.3 ± 0.8 m at ~10 ka BP, at -20.0 ± 0.8 m at ~9.2 ka BP, and at −15.1 ± 1.5 m at ~8.2 ka BP. Mid-Holocene index points indicate a continuous rise in RSL that, at ~7.1 ka BP and at ~6.0 ka BP, was at -8.3 ± 1.5 m and at −7.6 ± 0.8 m, respectively. Between 5 and 4.5 ka BP, limiting points constrain the RSL below −4.1 and above -4.6 m. There is a lack of data-points between 4.5 and 1.8 ka BP. Younger basal index points indicate a RSL stillstand at ~−2.8 m between ~1.7 and ~1.2 ka BP. The younger intercalated index point suggests RSL was still at −2.5 ± 0.7 m at ~0.8 ka BP.

5.19. Mid-eastern Adriatic Sea (#19)

The RSL history of the mid-western Adriatic Sea is restricted to the last ~2.6 ka BP. The database is composed of 23 index points and 1 limiting point. Data come from *Lythophyllum byssoides* samples and archaeological surveys performed on the islands of Vis and Bisevo in Croatia (Fig. 11, #19). The oldest index point places the RSL at -1.5 ± 0.3 m at ~2.6 ka BP. One archaeological index point indicates that RSL rose to -1.1 ± 0.3 m at ~1.9 ka BP. Multiple index points place the RSL at −0.7 ± 0.3 m between ~1.4 and ~1.1 ka BP and at -0.3 ± 0.3 m between ~0.6 and ~0.2 ka BP.

5.20. Mid-western Adriatic Sea (#20)

The RSL history for the mid-western Adriatic Sea (Fig. 11, #20) is composed of 3 index points and 3 limiting points from the coastal plain of Pescara and the lower Sangro river valley. At ~10.4 ka BP, RSL was lower than −18.6 m. The oldest intercalated index point places the RSL at -11 ± 0.6 m at ~7.7 ka BP. RSL rose to −7.4 ± 1.1 m at ~7.7 ka BP. A lack of index points did not allow us to properly assess the RSL in the last ~7.5 ka BP. The youngest limiting point indicates that RSL was above -3 m ~2.5 ka BP.

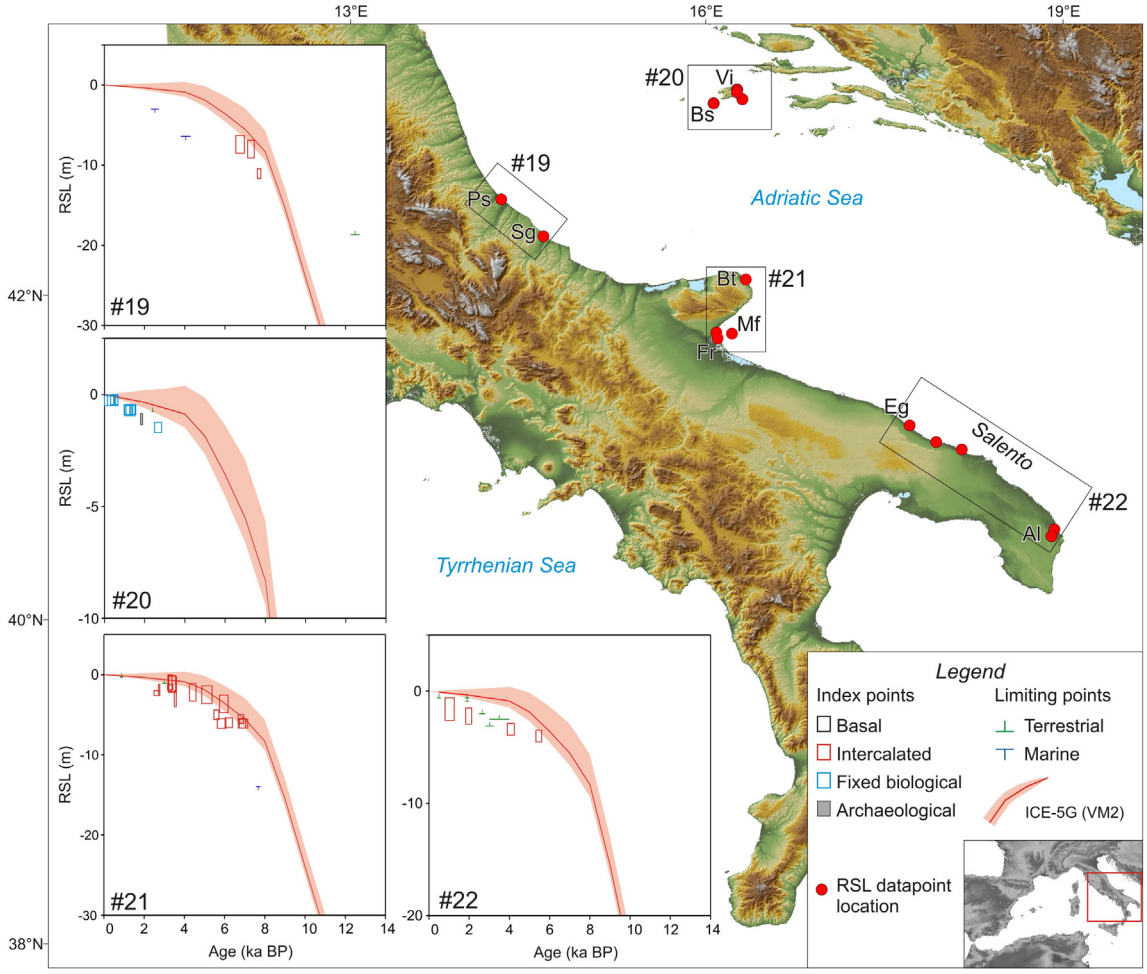

Fig. 11. RSL history in mid-eastern Adriatic Sea (#19), mid-western Adriatic Sea (#20), northern Apulia (#21) and southern Apulia (#22). Index points (boxes) are plotted as calibrated age against change in sea level relative to the present. Limiting points are plotted as terrestrial or marine horizontal lines. Dimensions of boxes and lines for each point based on 2s elevation and age errors. The relative sea-level data are compared to a prediction (red line with minimum and maximum errors) from the SELEN model (see Section 4). Red dots represent the approximate location of RSL data-points. Vi, Vis Island; Bs, Bisevo Island. Ps, Pescara coastal plain; Sg, Sangro coastal plain; Bt, Battaglia lake; Mf, Gulf of Manfredonia; Fr, Frattarolo lagoon. Eg, Egnazia; Al, Alimini piccolo lake.

5.21. Northern Apulia (#21)

The RSL history spans the mid to late Holocene. The database comprises 16 index points and 3 limiting points from cores in Battaglia coastal lake and Frattarolo marsh as well as from offshore cores in Gulf of Manfredonia (Fig. 11, #21). The oldest limiting point place the RSL above -14 m at ~7.7 ka BP. Multiple index points indicate RSL was at ~−6.0 m at ~6.8 ka BP. There is a scatter in the younger mid-Holocene index points, most likely due to compaction. At ~4.4 ka BP, RSL was at -2.2 ± 1.0 m. Then, multiple index points indicate RSL rose to ~−1.5 m. Younger index and limiting points, most likely affected by compaction, indicate that RSL rose to within ~2 m of modern MSL from ~2.6 ka BP to present.

5.22. Southern Apulia (#22)

The database is composed of 4 index points and 6 limiting points from lagoon cores in Alimini coastal lake and archaeological surveys carried out in the ancient towns of Egnazia and the Salento coast (Fig. 11, #22). The RSL history is restricted to the mid to late Holocene. At ~5.5 ka BP, RSL was at -4.0 ± 0.5 m. Then RSL rose to −3.4 ± 0.5 m at ~5.5 ka BP ~4.0 ka BP. Between ~4.0 and ~3.0 ka BP, RSL remained below ~−2.5 m. At ~2.0 ka BP, one intercalated index point places the RSL at −2.2 ± 0.7 m. RSL was still at −1.6 ± 1.0 m at ~1.0 ka BP.

6. Discussion

6.1. Standardization of the database and its applicability

We reconstructed the RSL histories of the western Mediterranean using an innovative multi-proxy standardization methodology based on: (1) modern taxa assemblages in Mediterranean lagoons and marshes; (2) beachrock characteristics (cement fabric, chemistry and sedimentary features); and (3) the modern distribution of Mediterranean fixed biological indicators on rocky coasts. We further added sea-level data derived from archaeological coastal structures (Auriemma and Solinas, 2009; Morhange and Marriner, 2015). Results indicate a generally good match between the different proxies in most of the regions included in the database. For example, in southern France there is very good agreement between the lagoonal index points and the virtually incompressible samples (i.e. *L. byssoides* and archaeological index points, Fig. 12A) for the last 2 ka. Similarly, lagoonal and beachrock index points are in good agreement with terrestrial and marine limiting points in documenting the RSL fall after the mid-Holocene highstand in southern Tunisia (Fig. 12B). At the basin scale, compaction free index points are above those samples that may have experienced compaction processes (Fig. 5A). Most basal index points have ages comprised between 7 and 5 ka BP (Fig. 5A), corresponding to the global slowdown in rates of rise and the onset of major coastal progradation (Anthony et al., 2014; Lambeck et al., 2014).

A major issue in sea-level studies is to understand how small scale RSL changes are manifest in coastal sedimentary sequences (e.g., Kemp et al., 2011; Gehrels and Shennan, 2015). In our database, marsh and lagoonal index points represents the majority of data. However, the vertical error bars of these index points remain too large to capture sub-millennial RSL variability in the microtidal setting of the Mediterranean Sea. To this end, methodological developments of the transfer function (e.g. Juggins and Birks, 2012) offer the potential for high-resolution sea-level reconstructions (e.g., Gehrels, 2000; Kemp and Telford, 2015). The identification of small-scale bio-stratigraphic changes from coastal sedimentary sequences and the development of regional predictive plant zonation-, foraminifera- and/or ostracod-

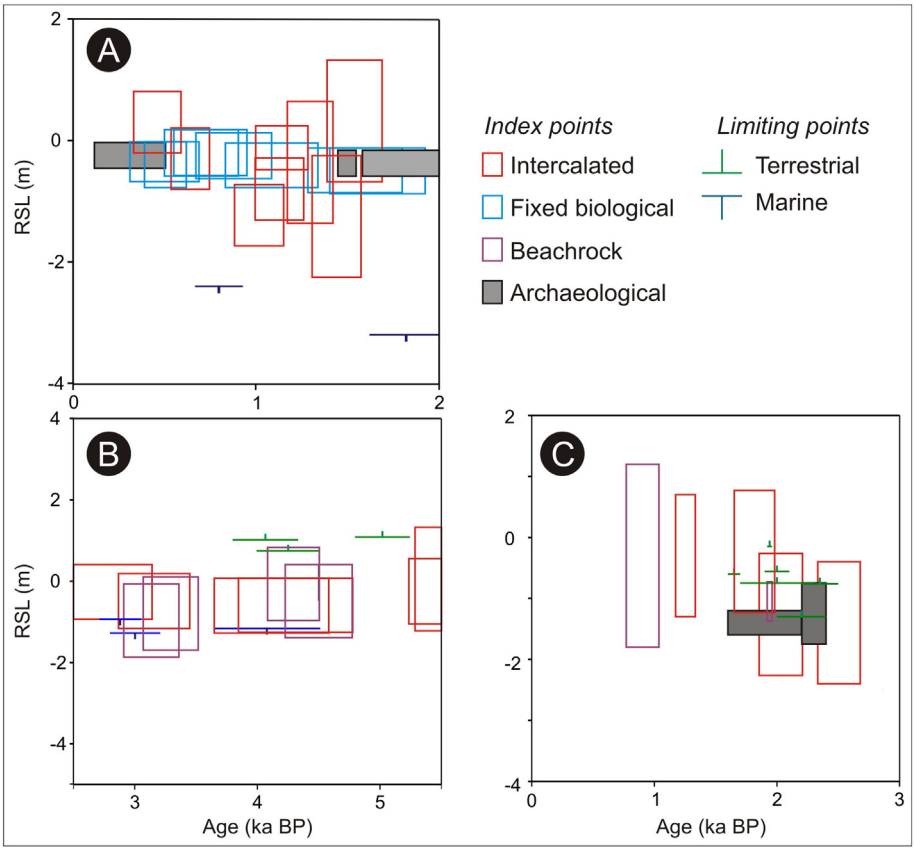

Fig. 12. Example of the applicability of the proposed multiproxy standardization in central France (A), southern Tunisia (B), and southwestern Sardinia (C). Index points (boxes) are plotted as calibrated age against change in sea level relative to present. Limiting points are plotted as terrestrial or marine horizontal lines. The dimensions of boxes and lines for each point are based on 2s elevation and age errors.

based transfer functions to reconstruct former sea-levels are seldom reported in the Mediterranean (e.g., Anadón et al., 2002; Silvestri et al., 2005; Triantaphyllou et al., 2005). This is mainly due to the microtidal setting of most Mediterranean coasts, which is not conducive to establishing a well-defined intertidal zoning. However, our results indicate the potential of inner or semi-enclosed lagoon samples as RSL index points in the Mediterranean Sea. In this database, we assigned an indicative range of 0 to -1 m MSL to these samples, on the basis of the available literature. Future development of local or regional transfer functions could significantly reduce this vertical uncertainly, possibly making them a high-resolution RSL indicator.

Our compilation underlines the importance of *L. byssoides* fossil rims as sea-level index points in the Mediterranean. The majority of our samples, collected at the beginning of the 1990s, show a large chronological error bar due to ^{14}C dating uncertainty. Recent developments in AMS techniques, pretreatment and calibration (e.g., Bronk Ramsey, 2008) could drastically reduce these uncertainties (e.g., Faivre et al., 2013).

Mediterranean beachrocks can be considered precise indicators when they are corroborated by chemical and fabric information of the cement and, when possible, by the description of sedimentary structures (Mauz et al., 2015b). Without such information, the resolution of beachrocks index points decreases considerably, making them a weak proxy for Mediterranean sea-level reconstruction. As an example, in southwestern Sardinia (#8), the large error bars of the youngest beachrock index point did not significantly improve the late Holocene RSL history of the region (Fig. 12C). Microstratigraphic analysis of the cement of these samples may lead to a considerable reduction in the error bar and, therefore, result in a better understanding of the RSL changes in this area.

Our database further confirmed the importance of archaeological RSL data-points. We decided to only produce index points from coastal structures closely related to former sea-level (i.e. fishtanks, fish ponds and ancient harbour interface structures such as quays and jetties). When coupled with fixed biological indicators, these structures may produce index points with uncertainty only represented by the leveling and the tidal errors (Morhange and Marriner, 2015). Conversely, we produced limiting points with such coastal structures whose relation with former sea-level is less clear (i.e. coastal quarries, roads, tombs, wrecks, sewage).

Our multi-proxy approach provides new insights into the ongoing debate about sea-level position during Roman times in the Tyrrhenian Sea. Fish tank interpretations by Evelpidou et al. (2012) place RSL between −0.58 and −0.32 m MSL while Lambeck et al.'s (2004b) interpretation places RSL between −1.37 and −1.2 m. On the Tiber Delta, Goiran et al. (2009, 2010) placed the RSL at -0.8 ± 0.2 m MSL at ~2.0 ka BP on the basis of the fixed biological indicators found in the Roman habour of Claudius' basin and the Darsena (Fig. 7, #9). One salt-marsh index point from the Tiber Delta indicates RSL was at -0.6 ± 0.6 m at ~1.9 ka BP (Di Rita et al., 2010). Long term uplift rates of ~0.11 mm a^{-1} are reported in the Tiber Delta area (Ferranti et al., 2010; Marra et al., 2013). If we apply the uplift correction to the two latter data-points we obtain a RSL of between −0.8 and −1 m MSL during Roman times. This value is similar (with errors) to the Roman RSL obtained in the Gulf of Gaeta (#10). Here, one lagoonal index point places the RSL at -1 ± 0.5 m at 2.1 ka BP. In summary, our database seems to suggest that RSL rose to within 1 m of modern MSL from ~2.0 ka BP to present. Nonetheless, the associated error bars do not allow us to reconcile the different functional and architectural interpretations of Roman fish tanks. Further high-resolution studies are required in this area, if possible that couple fixed biological indicators and archaeological coastal structures.

6.2. Predicted vs observed RSL changes in the western Mediterranean

There is a generally good qualitative agreement between the predicted and the observed RSL changes. In regions where the record extends from the early Holocene, the database documents rapid rising rates (≤8 mm a^{-1}) between ~12 and ~7.5 ka BP corresponding to the major deglaciation phase (e.g., Peltier, 2004; Lambeck et al., 2014). Rising rates significantly slowed in the remaining part of the mid-Holocene and reached values <1 mm a^{-1} during the late Holocene where ice equivalent meltwater input is negligible (Milne et al., 2005; Church et al., 2008). Comparison between predicted and observed RSL changes are only robust at those sites where the RSL reconstruction is mainly based on virtually incompressible and basal data points. Conversely, caution is required for comparisons done with RSL reconstructions based only on intercalated samples.

The database documents a general overestimation of the nominal ICE-5G (VM2) model prediction in most of the regions. This is not surprising since the ICE-5G (VM2) model was not constrained by RSL observations from far-field sites with respect to the formerly glaciated regions (Peltier, 2004), such as the Mediterranean Sea. Data from most of the regions located in the northwestern sectors of our database (#2, #3, #4, #5, #6, Figs. 6 and 7) and from northwestern Sicily (#12, Fig. 9) are in good agreement with the lower boundary of the predicted curve (i.e. between nominal and minimal, see Section 4, Table 2). Disparities increase eastwards and southwards where the minimal curve slightly overestimates the RSL position, notably in the Ionian and mid to southern Adriatic Seas (Figs. 9, #14 and 11).

Such underestimation is also visible in regions considered tectonically stable. However, sediment compaction cannot account for this misfit. For instance, the underestimation is also present in the mid-eastern Adriatic region where the database is only composed of virtually incompressible samples (Fig. 11, #19). It is possible that the chronology of the GIA model adopted in this study (and its rheological profile) could be modified in order to provide a better fit with the new RSL index points. However, we did not pursue this goal, since modifying these parameters would probably disrupt the agreement between the RSL observations available from polar regions and modelling predictions. This would require the implementation and the adoption of a fully 3D GIA model accounting for the lateral variations in viscosity, between the shield area and the remote sites, which is not the purpose of this study.

In our database, we avoided RSL reconstructions in areas affected by major tectonic deformation such as the Calabrian arc (see Section 2.1, Ferranti et al., 2006; Antonioli et al., 2009). However, comparison between predicted and observed RSL gave new insights into the influence of mild but significant long-term uplift on the sea-level history of a number regions. In mid-eastern Siciliy (region #13) our record agreed, using a larger dataset, with the results of previous studies (Dutton et al., 2009; Spampinato et al., 2011) that are consistent with long-term uplift rates of between ~0.4 and ~0.7 mm a^{-1}. In the western Ligurian Sea (region #4), the Holocene data-points collected near Nice describe a RSL history higher than those of the remaining areas of the region. The elevation of these data suggests that the low long-term uplift (average rate ≤0.06 mm a^{-1} since the last interglacial) reported by Dubar et al. (2008) has been active for more than half of the Holocene because these data are above the nominal curve from ~12.5 to ~5.5 ka BP. Our compilation confirms that such an uplift trend is restricted to the Nice area and rapidly decreases in the surrounding sectors, as already hypothesized on the basis of the MIS 5e elevations (Dubar et al., 2008; Rovere et al., 2011). Similarly, in the Tiber Delta (region #9) and on the Sele coastal plain (region #11) the long-term uplift rates reported by Ferranti et al. (2006, 2010) most likely control the position of RSL data points, especially for the early-to mid-Holocene. The offset between predictions and observations in central Spain (Fig. 6, #1) remains an open issue. Here, the early to mid-Holocene RSL data-points placed above the nominal curve suggest an underestimation of the RSL position by the ICE- 5G (VM2) isostatic model. At ~8.3 ka the RSL was ~6 m higher than in northern Spain (Fig. 6, #1). On-going vertical movements (Serpelloni et al., 2013) do not exceed ± 0.5 mm a^{-1} with slightly higher subsidence rates (<2 mm a^{-1}) near Valencia (Fig. 2); these data meant

that it was difficult to robustly support a tectonic component in the current elevation of the index points. However, the RSL record in this region is based on a restricted number of index and limiting points and further investigations are required to better assess the mid to late-Holocene evolution of this area.

Furthermore, our database indicates that the major western Mediterranean subsidence trends are recorded in the Ebro Delta and the northwestern Adriatic Sea. The comparison between the elevation of the index points from the Ebro Delta and the predicted RSL changes (Fig. 6, #2) indicates subsidence rates of ~1 mm a^{-1} between ~6.0 and ~3.5 ka BP, rising to ≥ 2 mm a^{-1} during the last ~2.5 ka BP. This subsidence pattern is chiefly controlled by the increase in sediment loading following the RSL stabilization at ~7.0 ka BP. The increasing subsidence rates recorded in the last ~2.5 ka BP are most likely linked to the transition from estuarine to deltaic environments at the river-mouth (Törnqvist, et al., 2008; Maselli and Trincardi, 2013) with a consequent increase of sediment loading. Furthermore, recent studies in Mediterranean deltaic contexts have revealed a negative correlation between subsidence rates and time, translating the rapid compaction of the latest Holocene deposits. Compaction rates progressively decline with the increasing age of sediments (Marriner et al., 2012a). The mechanistic explanation for this pattern appears consistent with the rapid compaction of the youngest delta sediments that undergo the most important phase of volume loss, through dewatering and oxidation of organic material, during earlier periods following deposition (Becker and Sultan, 2009).

Our data corroborated, using a larger dataset, the general subsidence trend in the northwestern portion of the Adriatic Sea (Fig. 10, #16, #18) already reported by Antonioli et al. (2009). South of the Po Delta, the observed subsidence is the sum of sediment compaction and long-term negative vertical motions related to the neotectonic framework of the area (e.g., Ferranti et al., 2006; Antonioli et al., 2009). Comparison between the elevation of basal and intercalated index points from the same area (and thus with comparable tectonics), gives insights into the compaction-related subsidence. We attempted this comparison in Codigoro and Comacchio (Appendix A, Cibin and Stefani, 2009; Sarti et al., 2009) and the calculated subsidence rates are ~0.5 mm a^{-1} for the last ~9.5 ka BP.

Human-induced subsidence explains the significant scatter in the index points from Venice lagoon (region #16, Fig. 10) especially during the last 2.0 ka (Serandrei-Barbero et al., 2006; Antonioli et al., 2009). In general, an assessment of the variability in subsidence trends in the northwestern sector of the Adriatic Sea is challenging. A comparative study, using de-compacted coring data, long-term vertical movements and the geometry of local faults would significantly improve the understanding of the Holocene RSL evolution of this area.

There is a small shift in the RSL curve between the eastern border of the Rhone Delta and the remaining sites of southern France (region #3, Fig. 6). The Rhone river shows major progradation rates (≥150 m a^{-1}) during the last 1.7 ka BP leading to significant sediment loading, especially on the eastern part of the delta (Maselli and Trincardi, 2013). However, some localized tectonic subsidence has been evoked as a cause for this peculiar RSL pattern (Vella and Provansal, 2000; Vella et al., 2005). These authors excluded compaction-related subsidence because most of the index points are basal peat samples that directly overlie the uncompressible Pleistocene substratum. Nonetheless, whether it is local tectonics or major sediment loading that has caused the subsidence, the eastern Rhone data-points are not indicative of the RSL history of southern France.

An intriguing open issue is represented by the RSL history of region #7 (northern Sardinia and southern Corsica, Fig. 7) and #8 (southwestern Sardinia, Fig. 8). Here, both lagoonal and beachrock index points are placed significantly below the minimal predicted curve, especially for the mid-Holocene. Both islands are considered to have been tectonically stable since the last interglacial (Ferranti et al., 2006) and ongoing vertical movements are negligible (Serpelloni et al., 2013). As for the mid-southern Adriatic and Ionian Seas, the underestimation of the isostatic contribution in this area may be a good explanation for the misfit between RSL index points and the predicted curve. However, in the early and mid Holocene, the sole index point from Is Mistras closely matches the RSL prediction (Fig. 8, #8) while lagoonal index points from Cagliari and Oristano (Antonioli et al., 2007) are significantly lower than the minimal predicted curve. Such a misfit could be related to some dating problems (both in Is Mistras and in Cagliari) or with compaction (even if the early Holocene record is based on beachrocks and basal samples). At the moment, we cannot robustly assess the mid to early Holocene RSL history in this sector of the western Mediterranean and additional datapoints are required.

Similarly, in region #7, beachrock samples (virtually incompressible) are found significantly lower than the predicted curve, between ~2 and ~7.1 ka BP. Here, the magnitude of the misfit (significantly greater than the remaining regions, especially in the Tyrrhenian Sea) calls for alternative explanations mainly focused on the quality of the RSL datapoints. Disparities arising from radiocarbon dates of beachrock bulk cement are not unusual (e.g., Vousdoukas et al., 2007), especially for samples during the early 1980s (like most of the beachrock of this region, Nesteroff, 1984). Results of recent coring in the Gulf of Sagone (mid-eastern Corsica) placed the RSL above -2.7 m MSL at ~3.8 ka BP and indicate that sea-level rise in the last ~2.5 ka BP was within 1 m (Ghilardi, 2015). These data suggest RSL was significantly higher than the one indicated by the beachrock samples, at least during the late Holocene.

As stated at the beginning of this section, the combined effects of glacio and hydro isostatic components in the western Mediterranean resulted in a continuous rise in RSL during the Holocene.

The sole exception is represented by the mid-Holocene highstand in southern Tunisia (Gulf of Gabes) that, according to our record, occurred between ~6.0 and ~5.0 ka BP and did not exceed 1.5 m above MSL. However, Morhange and Pirazzoli (2005), on the basis of ^{14}C dating of a subtidal shell (*Petricola* sp.) and vermetus (*Vermetus triqueter*), suggest a highstand at ~1.9 m during the same period. More recently, OSL dating of a beachrock outcrop in the Gulf of Gabes suggested a RSL at 1.4 ± 0.4 m MSL at ~6.0 ka BP (Mauz et al., 2015a). This estimate, coupled with our result, seems to suggest that the magnitude proposed by Morhange and Pirazzoli (2005) is slightly overestimated and may be affected by levelling errors with respect to the biological MSL.

Both the absence of significant historical seismicity and the long-term tectonic stability (Fig. 2) suggest that the southern Tunisia highstand is purely of isostatic origin (Stocchi et al., 2009; Mauz et al., 2015a). The geomorphology of the inner part of the Gulf of Gabes and the continental levering effects (e.g. the extensive upward deflection of continental interiors and the broad subsidence of ocean basin, Mitrovica and Milne, 2002) play a key role in the occurrence of this highstand. In fact, due to the wide and shallow (≤30 m depth) continental shelf (Sammari et al., 2006), the inner part of the Gulf of Gabes acts as a pure continental margin where the levering effects are not counterbalanced by the ocean loading. Thus, the subsidence driven by the water loading in the remaining part of the western Mediterranean is not able to offset the highstand in this region.

The timing of this highstand (~5.5 ka BP) suggests a negligible role of Northern hemisphere ice sheets due to the mutual cancellation of the meltwater contributions from the Laurentide and Fennoscandian ice sheets after ~7 ka BP (Stocchi and Spada, 2009; Stocchi et al., 2009). Conversely, our record improved and refined the RSL reconstruction provided by Stocchi et al. (2009) and Mauz et al. (2015a) confirming that the Tunisian high-stand is compatible with the melting history of the remote Antarctica ice sheet (Bentley, 1999; Stocchi and Spada, 2009; Stocchi et al., 2009).

6.3. RSL variability along the western Mediterranean basin

In order to better assess the spatial variability of Holocene RSL changes along the western Mediterranean basin, we tried to minimize both the local vertical movements and the effects of compaction in

our database. For this reason, Fig. 13A,C only depicts the index points collected at sites: (i) with long-term vertical movements ≤0.06 mm a^{-1} (Fig. 2, MIS 5e); (ii) with ongoing vertical motions between -0.5 and 0.5 mm a^{-1} (Fig. 2, GPS); and (iii) not affected by significant compaction-related subsidence (e.g., the Ebro Delta) or local fault activity (e.g. the Var fault).

With the sole exception of southern Tunisia, the data indicate a continuous rise in RSL which, at the basin scale, rose by ~45 m in ~12 ka (Fig. 13A).

Even if affected by scatter, the data show a general slowdown in western Mediterranean sea-level rise starting from ~7.5 ka BP, consistent with the final phase of the North American deglaciation (e.g., Carlson et al., 2008; Lambeck et al., 2014) followed by a further decrease in rising rates related to the progressive reduction in meltwater input (e.g., Peltier and Tushingham, 1991; Milne et al., 2005).

Comparatively, the late Holocene record (i.e. the last 4 ka BP) is affected by less scatter. In this period, ice equivalent meltwater input is negligible (Peltier, 2004; Milne et al., 2005; Church et al., 2008). Therefore, once tectonics and sediment compaction are factored out, any change observed in RSL is entirely related to vertical land movements due to GIA (e.g., Engelhart et al., 2009, 2015). According to Engelhart et al., 2009, we calculated the late Holocene RSL rising rates excluding the 20th century sea-level contribution and thus expressing all our data with respect to MSL at A.D. 1900 (Fig. 13B). We further excluded for this analysis the southern Tunisia index points describing a RSL history not comparable with the other datasets in our study area (see Section 6.2). Thus, the late Holocene record in Fig. 13B most likely encompasses the total variability in isostatic contribution in the western Mediterranean. Our estimates indicate that GIA-related land movements in the western Mediterranean vary between ~3.4 m in the southeastern part of the basin up to ~1.6 m in the northwest. The latter value is mainly derived from region #14 and #22, where the Holocene record is only based on intercalated index points. For this reason, assessment of any possible role of compaction in the late Holocene was not possible with the present dataset.

Preliminary analysis of the normal distribution of late Holocene rising rates (Fig. 4D) shows that values ranging between 0.55 and 0.20 mm a^{-1} are the most represented along the Mediterranean coast. Rates increase up to ~0.85 mm a^{-1}, but caution should be used in using these values because a possible compaction influence cannot be excluded in some dataset from the southeastern sector of the western Mediterranean Sea (see above).

The Fig. 13D clearly shows that late Holocene sea-level rising rates are slower than those recorded by most of the Mediterranean tide gauges (Table 3) but still account for at least the 25-30% of the rate. Therefore, for better understanding of current rates of Mediterranean sea-level rise from tide gauges, correction for GIA is required (e.g., Engelhart et al., 2009; Church and White, 2011). Site-specific assessment of the GIA signal in the western Mediterranean is beyond the scope of this paper. However, future application of spatio-temporal statistical models (e.g., Parnell et al., 2011; Engelhart et al., 2015; Parnell and Gehrels, 2015) to the Mediterranean RSL data may provide a long-term baseline against which to gauge changes in sea-level during the 20th century (e.g., Engelhart et al., 2009; Kemp et al., 2011; Gehrels and Woodworth, 2013) and provide a framework for more accurate 21st century sea-level predictions (e.g. Church and White, 2011; Horton et al., 2014).

7. Conclusions

In this paper, we reviewed 917 RSL proxies using, for the first time in the Mediterranean basin, a standardized protocol to produce RSL index and limiting points. This allowed us to compare and contrast data from different literature sources in order to obtain basin-scale insights into the processes driving Holocene RSL changes. The database in Appendix A is dynamic and future users can add further data or subdivide the data

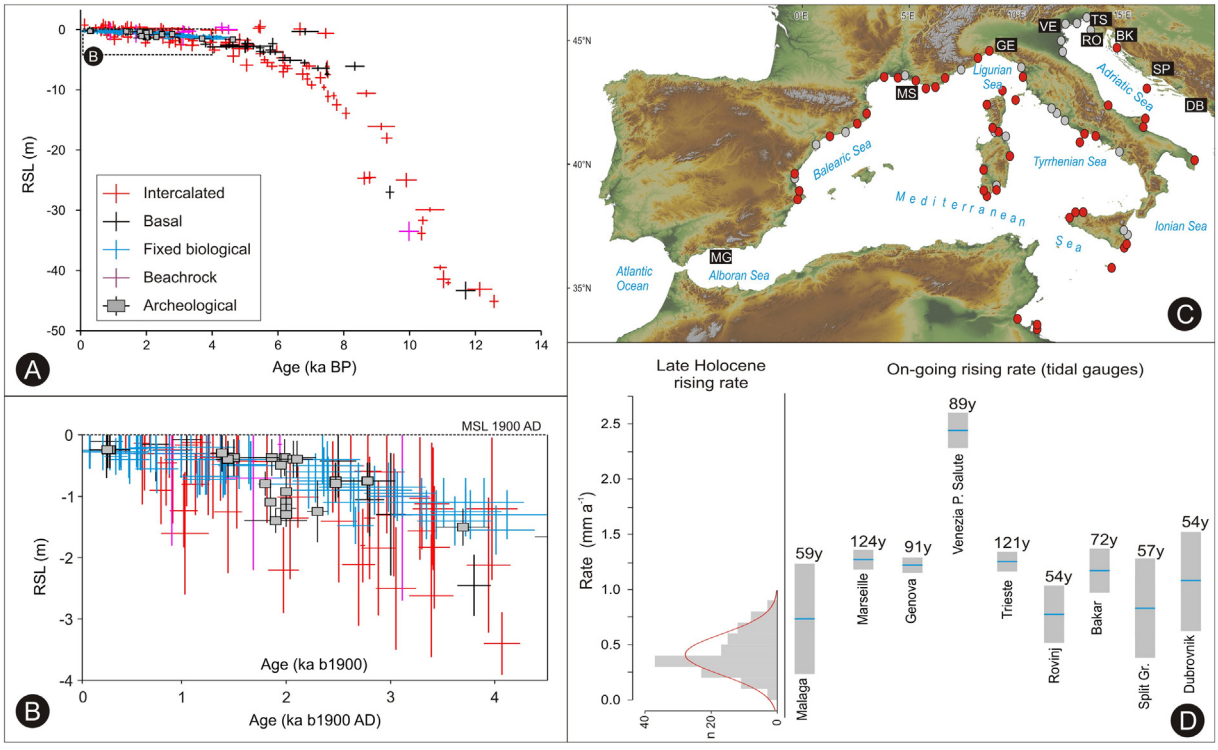

Fig. 13. A) Total plot of the western Mediterranean index points from areas that are tectonically stable and minimally affected by compaction-related subsidence. B) Variability of late Holocene (last 4.0 ka BP) RSL index points in the western Mediterranean. Note that the x and y axis are forced to the MSL at A.D. 1900. C) Approximate location of the index points plotted (red dots) and not plotted (gray dots) in panel a, see Section 6.3 for details. D) Normal distribution of late Holocene rising rates plotted against the 20th century RSL rise (with error) derived from long-term Mediterranean tidal gauges (see Table 3). Number above squares denotes the number of years used to compute the trend. MG, Malaga; MS, Marseille; GE, Genova; VE, Venezia P. Salute; TR, Trieste; RO, Rovinj; BK, Bakar; SP, Split Gradska; DB, Dubrovnik.

Table 3
Ongoing sea-level rise rates recorded by long-term (>50 years) tide gauges in the western Mediterranean (source, PMSL, access date, 22/02/2016, http://www.psmsl.org/products/trends/trends.txt).

Tidal station	Lat.	Long.	Years of measurements	Rate mm a^{-1}	Error mm a^{-1}
Genova	44.4	8.9	1884–1996	1.20	0.07
Marseille	43.27	5.35	1885–2012	1.29	0.13
Trieste	45.64	13.75	1875–2012	1.26	0.10
Venezia P. Salute	45.43	12.33	1909–2000	2.47	0.26
Bakar	45.3	14.53	1930–2011	1.17	0.27
Malaga	36.71	−4.41	1944–2012	0.71	0.66
Split Gradska	43.5	16.44	1953–2011	0.84	0.50
Dubrovnik	42.65	18.06	1956–2010	1.10	0.42
Rovinj	45.08	13.62	1956–2011	0.76	0.42

points on the basis of other criteria. Moreover, future RSL reconstructions carried out using this standardized methodology will produce homogeneous and comparable RSL data rendering the assessment of RSL variability in the Mediterranean much easier.

Our quality-controlled database has an excellent temporal coverage, allowing a robust reconstruction of RSL changes since 14 ka BP. By contrast, the spatial coverage is significantly affected by a paucity of RSL data from the southern coast of the Mediterranean. Therefore, future sea-level investigations in Algeria, Morocco and particularly Libya (a key site for tuning the global eustatic signal, e.g., Milne and Mitrovica, 2008) are a key priority. Thanks to the very local RSL highstand of the Gulf of Gabes, we were able to detect the influence of the remote Antarctic ice sheet on the Mediterranean RSL history. In the remaining part of western Mediterranean, GIA (glacio- and hydro-) induced subsidence that prevented the occurrence of this highstand, with a continuous rise in RSL for the whole Holocene. Our data indicate a sudden slowdown in the rising rates at ~7.5 ka BP and a further deceleration during the last ~4.0, where any observed changes are related to variability in GIA or neotectonics.

Precise estimates of Mediterranean sea-level rise in the pre-satellite era are essential for accurate 21st century sea-level predictions, but the use of tide-gauge records is complicated by the contributions from changes in land level due to GIA. In this paper, we provide a preliminary quantification of the on-going GIA contribution in the western Mediterranean that, at least in the northwestern sector, accounts for the 25-30% of the on-going rising rates recorded by the tidal gauges. In the southeastern sector, our results weakly constrained the GIA contribution because the sole presence of intercalated index points did not allow for a robust late Holocene RSL reconstruction. Improvement of this dataset and future applications of spatio-temporal statistical techniques are required for site-specific estimates of the isostatic contribution and for the consequent improved assessment of 20th century acceleration of Mediterranean sea-level rise.

Supplementary data to this article can be found online at http://dx.doi.org/10.1016/j.earscirev.2016.02.002.

Acknowledgments

This work has been carried out thanks to the support of the Labex OT-Med (ANR-11-LABX-0061) and of the A*MIDEX project (no ANR-11-IDEX-0001-02), funded by the "Investissements d'Avenir" program of the French National Research Agency (ANR). This compilation of the database was motivated by discussions at the workshops of Medflood, INQUA project n. 1203 and PALSEA (PAGES/INQUA/WUN working group). GS has been supported by the DiSBeF grant n. CUP H31J13000160001. AF was supported by University of Padova (project n° C91J10000320001). AR's research is funded by the Institutional Strategy of the University of Bremen, German Excellence Initiative, and by ZMT Center for Tropical Marine Ecology.

MV would like to thank Prof. Ben Horton (Sea Level Research, Rutgers University, USA), Prof. Edouard Bard (Collège de France-CEREGE, France) and Prof. Bruno Hamelin (Aix Marseille Université-CEREGE, France) for the fruitful discussions. We thank Veronica Rossi (University of Bologna, Italy), Stefano Furlani (University of Trieste, Italy), Pilàr Carmona-Gonzàles (University of Valencia, Spain), Matthieu Ghilardi (CNRS-CEREGE, France), Marco Firpo and Pierluigi Brandolini (University of Genova, Italy), Daniela Pantosti and Paolo Marco De Martini (INGV Rome, Italy) for their help in the compilation of the database and the definition of the indicative meanings. The constructive comments of the associate editor I. Candy and of the two anonymous reviewers significantly improved an earlier version of the paper.

References

Ambert, P., 1999. Les formations littorales Pléistocènes du Languedoc. Quaternaire 10, 83–93.
Amorosi, A., Dinelli, E., Rossi, V., Vaiani, S.C., Sacchetto, M., 2008a. Late Quaternary palaeoenvironmental evolution of the Adriatic coastal plain and the onset of Po River Delta. Palaeogeogr. Palaeoclimatol. Palaeoecol. 268 (1), 80–90.
Amorosi, A., Fontana, A., Antonioli, F., Primon, S., Bondesan, A., 2008b. Post-LGM sedimentation and Holocene shoreline evolution in the NW Adriatic coastal area. GeoActa 7, 41–67.
Amorosi, A., Ricci Lucchi, M., Rossi, V., Sarti, G., 2009. Climate change signature of small-scale parasequences from Lateglacial–Holocene transgressive deposits of the Arno valley fill. Palaeogeogr. Palaeoclimatol. Palaeoecol. 273 (1), 142–152.
Amorosi, A., Rossi, V., Vella, C., 2013. Stepwise post-glacial transgression in the Rhône Delta area as revealed by high-resolution core data. Palaeogeogr. Palaeoclimatol. Palaeoecol. 374, 314–326.
Anadón, P., Gliozzi, E., Mazzini, I., 2002. Paleoenvironmental Reconstruction of Marginal Marine Environments from Combined Paleoecological and Geochemical Analyses on Ostracods. In: J., Holmes, A., Chivas (Eds.), The Ostracoda: Applications in Quaternary Research. Geophysical Monograph vol. 131, pp. 227–247.
Anthony, E.J., Marriner, N., Morhange, C., 2014. Human influence and the changing geomorphology of Mediterranean deltas and coasts over the last 6000 years: from progradation to destruction phase? Earth Sci. Rev. 139, 336–361.
Antonioli, F., Anzidei, M., Lambeck, K., Auriemma, R., Gaddi, D., Furlani, S., Orrù, P., Solinas, E., Gaspari, A., Karinja, S., Kovacic, V., Surace, L., 2007. Sea-level change during the Holocene in Sardinia and in the northeastern Adriatic (central Mediterranean Sea) from archaeological and geomorphological data. Quat. Sci. Rev. 26 (19), 2463–2486.
Antonioli, F., Chemello, R., Improta, S., Riggio, S., 1999. The Dendropoma (Mollusca Gastropoda, Vermetidae) intertidal reef formations and their paleoclimatological use. Mar. Geol. 161, 155–170.
Antonioli, F., D'Orefice, M., Ducci, S., Firmati, M., Foresi, L.M., Graciotti, R., Principe, C., 2011. Palaeogeographic reconstruction of northern Tyrrhenian coast using archaeological and geomorphological markers at Pianosa island (Italy). Quat. Int. 232 (1), 31–44.
Antonioli, F., Ferranti, L., Fontana, A., Amorosi, A., Bondesan, A., Braitenberg, C., Dutton, A., Fontolan, G., Furlani, S., Lambeck, K., Mastronuzzi, G., Monaco, C., Spada, G., Stocchi, P., 2009. Holocene relative sea-level changes and vertical movements along the Italian and Istrian coastlines. Quat. Int. 206 (1), 102–133.
Antonioli, F., Lo Presti, V., Rovere, A., Ferranti, L., Anzidei, M., Furlani, S., Mastronuzzi, G., Orrù, P., Scicchitano, G., Sannino, G., Spampinato, C.R., Pagliarulo, R., Deiana, G., de Sabata, E., Sanso, P., Vacchi, M., Vecchio, A., 2015. Tidal notches in Mediterranean Sea: a comprehensive analysis. Quat. Sci. Rev. 119, 66–84.
Anzidei, M., Antonioli, F., Lambeck, K., Benini, A., Soussi, M., Lakhdar, R., 2011. New insights on the relative sea level change during Holocene along the coasts of Tunisia and western Libya from archaeological and geomorphological markers. Quat. Int. 232 (1), 5–12.
Anzidei, M., Lambeck, K., Antonioli, F., Furlani, S., Mastronuzzi, G., Serpelloni, E., Vannucci, G., 2014. Coastal structure, sea-level changes and vertical motion of the land in the Mediterranean. Geol. Soc. Lond., Spec. Publ. 388 (1), 453–479.
Auriemma, R., Solinas, E., 2009. Archaeological remains as sea level change markers: a review. Quat. Int. 206 (1), 134–146.
Bard, E., Hamelin, B., Arnold, M., Montaggioni, L., Cabioch, G., Faure, G., Rougerie, F., 1996. Deglacial sea-level record from Tahiti corals and the timing of global meltwater discharge. Nature 382 (6588), 241–244.
Bard, E., Hamelin, B., Delanghe-Sabatier, D., 2010. Deglacial meltwater pulse 1B and Younger Dryas sea levels revisited with boreholes at Tahiti. Science 327 (5970), 1235–1237.
Becker, R.H., Sultan, M., 2009. Land subsidence in the Nile Delta: inferences from radar interferometry. The Holocene 19, 949–954.
Bentley, M.J., 1999. Volume of Antarctic ice at the Last Glacial Maximum, and its impact on global sea level change. Quat. Sci. Rev. 18 (14), 1569–1595.
Billi, A., Faccenna, C., Bellier, O., Minelli, L., Neri, G., Piromallo, C., Presti, D., Scrocca, D., Serpelloni, E., 2011. Recent tectonic reorganization of the Nubia–Eurasia convergent boundary heading for the closure of the western Mediterranean. Bull. Soc. Géol. Fr. 182 (4), 279–303.
Blázquez, A.M., Usera, J., 2010. Palaeoenvironments and Quaternary foraminifera in the Elx coastal lagoon (Alicante, Spain). Quat. Int. 221 (1), 68–90.
Bronk Ramsey, C., 2008. Radiocarbon dating: revolutions in understanding. Archaeometry 50 (2), 249–275.
Caldara, M., Simone, O., 2005. Coastal changes in the eastern Tavoliere Plain (Apulia, Italy) during the Late Holocene: natural or anthropic? Quat. Sci. Rev. 24 (18), 2137–2145.

Caldara, M., Caroli, I., Simone, O., 2008. Holocene evolution and sea-level changes in the Battaglia basin area (eastern Gargano coast, Apulia, Italy). Quat. Int. 183 (1), 102–114.

Carboni, M.G., Bergamin, L., Di Bella, L., Esu, D., Cerone, E.P., Antonioli, F., Verrubbi, V., 2010. Palaeoenvironmental reconstruction of late Quaternary foraminifera and molluscs from the ENEA borehole (Versilian plain, Tuscany, Italy). Quat. Res. 74 (2), 265–276.

Carboni, M.G., Bergamin, L., Di Bella, L., Iamundo, F., Pugliese, N., 2002. Palaeoecological evidences from foraminifers and ostracods on Late Quaternary sea-level changes in the Ombrone river plain (central Tyrrhenian coast, Italy). Geobios 35, 40–50.

Carboni, M.G., Succi, M.C., Bergamin, L., Di Bella, L., Frezza, V., Landini, B., 2009. Benthic foraminifera from two coastal lakes of southern Latium (Italy). Preliminary evaluation of environmental quality. Mar. Pollut. Bull. 59 (8), 268–280.

Carlson, A.E., LeGrande, A.N., Oppo, D.W., Came, R.E., Schmidt, G.A., Anslow, F.S., Licciardi, J.M., Obbink, E.A., 2008. Rapid early Holocene deglaciation of the Laurentide ice sheet. Nat. Geosci. 1 (9), 620–624.

Carminati, E., Doglioni, C., Scrocca, D., 2003. Apennines subduction-related subsidence of Venice (Italy). Geophys. Res. Lett. 30 (13).

Carmona-González, P.C., Ballester, J.P., 2011. Geomorphology, Geoarchaeology and Ancient Settlement in the Valencian Gulf (Spain). Méditerranée. Revue géographique des pays méditerranéens/Journal of Mediterranean geography 117, pp. 61–72.

Church, J.A., White, N.J., 2011. Sea-level rise from the late 19th to the early 21st century. Surv. Geophys. 32 (4-5), 585–602.

Church, J.A., White, N.J., Aarup, T., Wilson, W.S., Woodworth, P.L., Domingues, C.M., Hunter, J.R., Lambeck, K., 2008. Understanding global sea levels: past, present and future. Sustain. Sci. 3 (1), 9–22.

Cibin U., Stefani, M., 2009. Carta Geologica d'Italia alla scala 1:50.000. Foglio 187, Codigoro. Note illustrative. http://www.isprambiente.gov.it/Media/carg/note_illustrative/187_Codigoro.pdf

Cimerman, F., Langer, M.R., 1991. Mediterranean Foraminifera. Slovenska Akademija Znanosti in Umetnosti, Ljubljana.

Colombaroli, D., Marchetto, A., Tinner, W., 2007. Long-term interactions between Mediterranean climate, vegetation and fire regime at Lago di Massaciuccoli (Tuscany, Italy). J. Ecol. 95 (4), 755–770.

Correggiari, A., Roveri, M., Trincardi, F., 1996. Late Pleistocene and Holocene evolution of the north Adriatic Sea. Il Quaternario 9, 697–704.

De Martini, P.M., Barbano, M.S., Smedile, A., Gerardi, F., Pantosti, D., Del Carlo, P., Pirrotta, C., 2010. A unique 4000 year long geological record of multiple tsunami inundations in the Augusta Bay (eastern Sicily, Italy). Mar. Geol. 276 (1), 42–57.

De Muro, S., Orrù, P., 1998. Il contributo delle Beach-Rock nello studio della risalita del mare olocenico. Le Beach-Rock post-glaciali della Sardegna nord-orientale. Il Quaternario 11 (1), 19–39.

Deschamps, P., Durand, N., Bard, E., Hamelin, B., Camoin, G., Thomas, A.L., Yokoyama, Y., 2012. Ice-sheet collapse and sea-level rise at the Bolling warming 14,600 years ago. Nature 483 (7391), 559–564.

Desruelles, S., Fouache, É., Ciner, A., Dalongeville, R., Pavlopoulos, K., Kosun, E., Coquinot, Y., Potdevin, J.L., 2009. Beachrocks and sea level changes since Middle Holocene: comparison between the insular group of Mykonos–Delos–Rhenia (Cyclades, Greece) and the southern coast of Turkey. Glob. Planet. Chang. 66 (1), 19–33.

Di Rita, F., Melis, R.T., 2013. The cultural landscape near the ancient city of Tharros (central West Sardinia): vegetation changes and human impact. J. Archaeol. Sci. 40 (12), 4271–4282.

Di Rita, F., Celant, A., Magri, D., 2010. Holocene environmental instability in the wetland north of the Tiber delta (Rome, Italy): sea-lake-man interactions. J. Paleolimnol. 44 (1), 51–67.

Di Rita, F., Simone, O., Caldara, M., Gehrels, W.R., Magri, D., 2011. Holocene environmental changes in the coastal Tavoliere Plain (Apulia, southern Italy): a multiproxy approach. Palaeogeogr. Palaeoclimatol. Palaeoecol. 310 (3), 139–151.

Dubar, M., Anthony, E.J., 1995. Holocene environmental change and river-mouth sedimentation in the Baie des Anges, French Riviera. Quat. Res. 43 (3), 329–343.

Dubar, M., Innocent, C., Sivan, O., 2008. Radiometric dating (U/Th) of the lower marine terrace (MIS 5.5) west of Nice (French Riviera): morphological and neotectonic quantitative implications. Compt. Rendus Geosci. 340 (11), 723–731.

Dumas, B., Guérémy, P., Raffy, J., 2005. Evidence for sea-level oscillations by the "characteristic thickness" of marine deposits from raised terraces of Southern Calabria (Italy). Quat. Sci. Rev. 24 (18), 2120–2136.

Dupré, M., Fumanal, M.P., Sanjaume, E., Santisteban, C., Usera, J., 1988. Quaternary evolution of Pego coastal lagoon (Southern Valencia, Spain). Palaeogeogr. Palaeoclimatol. Palaeoecol. 68, 291–299.

Dura, T., Cisternas, M., Horton, B.P., Ely, L.L., Nelson, A.R., Wesson, R.L., Pilarczyk, J.E., 2014. Coastal evidence for Holocene subduction-zone earthquakes and tsunamis in central Chile. Quat. Sci. Rev. 113, 93–111.

Dutton, A., Lambeck, K., 2012. Ice volume and sea level during the last interglacial. Science 337 (6091), 216–219.

Dutton, A., Scicchitano, G., Monaco, C., Desmarchelier, J.M., Antonioli, F., Lambeck, K., Mortimer, G., 2009. Uplift rates defined by U-series and 14 C ages of serpulid-encrusted speleothems from submerged caves near Siracusa, Sicily (Italy). Quat. Geochronol. 4 (1), 2–10.

Edwards, R.J., 2006. Mid-to late-Holocene relative sea-level change in southwest Britain and the influence of sediment compaction. The Holocene 16 (4), 575–587.

Engelhart, S.E., Horton, B.P., 2012. Holocene sea level database for the Atlantic coast of the United States. Quat. Sci. Rev. 54, 12–25.

Engelhart, S.E., Horton, B.P., Douglas, B.C., Peltier, W.R., Törnqvist, T.E., 2009. Spatial variability of late Holocene and 20th century sea-level rise along the Atlantic coast of the United States. Geology 37, 1115–1118.

Engelhart, S.E., Vacchi, M., Horton, B.P., Nelson, A.R., Kopp, R.E., 2015. A sea-level database for the Pacific coast of central North America. Quat. Sci. Rev. 113, 78–92.

Evelpidou, N., Pirazzoli, P., Vassilopoulos, A., Spada, G., Ruggieri, G., Tomasin, A., 2012. Late Holocene sea level reconstructions based on observations of Roman fish tanks, Tyrrhenian Coast of Italy. Geoarchaeology 27 (3), 259–277.

Faccenna, C., Becker, T.W., Auer, L., Billi, A., Boschi, L., Brun, J.P., Capitanio, F.A., Funiciello, F., Horvàth, F., Jolivet, L., Piromallo, C., Royden, L., Rossetti, F., Serpelloni, E., 2014. Mantle dynamics in the Mediterranean. Rev. Geophys. 52 (3), 283–332.

Faivre, S., Bakran-Petricioli, T., Horvatincic, N., 2010. Relative sea-level change during the Late Holocene on the Island of Vis (Croatia)–Issa Harbour Archaeological Site. Geodin. Acta 23 (5-6), 209–223.

Faivre, S., Bakran-Petricioli, T., Horvatinčić, N., Sironić, A., 2013. Distinct phases of relative sea level changes in the central Adriatic during the last 1500 years—influence of climatic variations? Palaeogeogr. Palaeoclimatol. Palaeoecol. 369, 163–174.

Farrell, W.E., Clark, J.A., 1976. On post-glacial sea level. R. Astron. Soc. Geophys. J. 46, 647–657.

Ferranti, L., Antonioli, F., Anzidei, M., Monaco, C., Stocchi, P., 2010. The timescale and spatial extent of vertical tectonic motions in Italy: insights from relative sea-level changes studies. J. Virtual Explor. 36 (Paper 30).

Ferranti, L., Antonioli, F., Mauz, B., Amorosi, A., Dai Pra, G., Mastronuzzi, G., Monaco, C., Orrù, P.E., Pappalardo, M., Radtke, U., Renda, P., Romano, P., Sansò, P., Verrubbi, V., 2006. Markers of the last interglacial sea-level high stand along the coast of Italy: tectonic implications. Quat. Int. 145, 30–54.

Ferranti, L., Monaco, C., Antonioli, F., Maschio, L., Kershaw, S., Verrubbi, V., 2007. The contribution of regional uplift and coseismic slip to the vertical crustal motion in the Messina Straits, Southern Italy: evidence from raised Late Holocene shorelines. J. Geophys. Res. Solid Earth 112 (B6).

Flemming, N.C., 1969. Archaeological evidence for eustatic change of sea level and earth movements in the western Mediterranean during the last 2000 years. Geol. Soc. Am. Spec. Pap. 109, 1–98.

Furlani, S., Antonioli, F., Biolchi, S., Gambin, T., Gauci, R., Lo Presti, V., Anzidei, M., Devoto, S., Palombo, M., Sulli, A., 2013. Holocene sea level change in Malta. Quat. Int. 288, 146–157.

Furlani, S., Biolchi, S., Cucchi, F., Antonioli, F., Busetti, M., Melis, R., 2011. Tectonic effects on Late Holocene sea level changes in the Gulf of Trieste (NE Adriatic Sea, Italy). Quat. Int. 232 (1), 144–157.

Gehrels, W.R., 2000. Using foraminiferal transfer functions to produce high-resolution sea-level records from salt-marsh deposits, Maine, USA. The Holocene 10 (3), 367–376.

Gehrels, W.R., Long, A.J., 2007. Quaternary land-ocean interactions: sea-level change, sediments and tsunami. Mar. Geol. 242, 169–190.

Gehrels, W.R., Woodworth, P.L., 2013. When did modern rates of sea-level rise start? Glob. Planet. Chang. 100, 263–277.

Gehrels, W.R., Shennan, I., 2015. Sea level in time and space: revolutions and inconvenient truths. J. Quat. Sci. 30 (2), 131–143.

Gerardi, F., Smedile, A., Pirrotta, C., Barbano, M.S., De Martini, P.M., Pinzi, S., Gueli, A.M., Ristuccia, G.M., Stella, G., Troja, S.O., 2012. Geological record of tsunami inundations in Pantano Morghella (south-eastern Sicily) both from near and far-field sources. Nat. Hazards Earth Syst. Sci. 12 (4), 1185–1200.

Ghilardi, M., 2015. Approche géoarchéologique des basses vallées fluviales de la Corse: la necessaire prise en compte de l'evolution paysagère au cours de l'Holocène. Rapport d'activités 2013–2014. Programme collectif de recherche (PCR 2013-2015) (112 pp.).

Goiran, J.P., Tronchère, H., Collalelli, U., Salomon, F., Djerbi, H., 2009. Découverte d'un niveau marin biologique sur les quais de Portus: le port antique de Rome. Méditerranée 1, 59–67.

Goiran, J.P., Tronchère, H., Salomon, F., Carbonel, P., Djerbi, H., Ognard, C., 2010. Palaeoenvironmental reconstruction of the ancient habours of Rome: Claudius and Trajan's marine habours on the Tiber delta. Quat. Int. 216 (1), 3–13.

Gravina, M.F., Ardizzone, G.D., Scaletta, F., Chimenz, C., 1989. Descriptive analysis and classification of benthic communities in some Mediterranean coastal lagoons (central Italy). Mar. Ecol. 10 (2), 141–166.

Hall, G.F., Hill, D.F., Horton, B.P., Engelhart, S.E., Peltier, W.R., 2013. A high-resolution study of tides in the Delaware Bay: past conditions and future scenarios. Geophys. Res. Lett. 40. http://dx.doi.org/10.1029/2012GL054675.

Hanor, J.S., 1978. Precipitation of beachrock cements: mixing of marine and meteoric waters vs. CO^2-degassing. J. Sediment. Res. 48, 489–501.

Herak, M., Herak, D., Markušić, S., 1996. Revision of the earthquake catalogue and seismicity of Croatia, 1908–1992. Terra Nova 8 (1), 86–94.

Higginbotham, J.A., 1997. Piscinae: Artificial Fishponds in Roman Italy. UNC Press Books.

Hijma, M., Engelhart, S.E., Tornqvist, T.E., Horton, B.P., Hu, P., Hill, D., 2015. A protocol for a Geological Sea-level Database. In: Shennan, I., Long, A., Horton, B.P. (Eds.), Handbook of Sea Level Research. Wiley, pp. 536–553.

Hill, D.F., Griffiths, S.D., Peltier, W.R., Horton, B.P., Törnqvist, T.E., 2011. High-resolution numerical modeling of tides in the western Atlantic, Gulf of Mexico, and Caribbean Sea during the Holocene. J. Geophys. Res. Oceans 116 (C10).

Hopley, D., 1986. Beachrock as a Sea-level Indicator. In: Van de Plassche, O. (Ed.), Sea-level Research: A Manual for the Collection and Evaluation of Data. Geo Books, Norwich, pp. 157–173.

Horton, B.P., Shennan, I., 2009. Compaction of Holocene strata and the implications for relative sea level change on the east coast of England. Geology 37 (12), 1083–1086.

Horton, B.P., Rahmstorf, S., Engelhart, S.E., Kemp, A.C., 2014. Expert assessment of sea-level rise by AD 2100 and AD 2300. Quat. Sci. Rev. 84, 1–6.

Jedoui, Y., Kallel, N., Fontugne, M., Ismail, H.B., M'Rabet, A., Montacer, M., 1998. A high relative sea-level stand in the middle Holocene of southeastern Tunisia. Mar. Geol. 147 (1), 123–130.

Jolivet, L., Faccenna, C., 2000. Mediterranean extension and the Africa–Eurasia collision. Tectonics 19 (6), 1095–1106.

Jolivet, L., Augier, R., Faccenna, C., Negro, F., Rimmele, G., Agard, P., Robin, C., Rossetti, F., Crespo-Blanc, A., 2008. Subduction, convergence and the mode of backarc extension in the Mediterranean region. Bull. Soc. Géol. Fr. 179 (6), 525–550.

Juggins, S., Birks, H.J.B., 2012. Quantiative Environmental Reconstructions from Biological Data. In: Birks, H.J.B., Lotter, A.F., Juggins, S., Smol, J.P. (Eds.), Data Handling and Numerical Techniques. Springer, pp. 431–494.

Kelletat, D., 2006. Beachrock as sea-level indicator? Remarks from a geomorphological point of view. J. Coast. Res. 1558–1564.

Kemp, A.C., Telford, R.J., 2015. Transfer functions. In: Shennan, I., Long, A., Horton, B.P. (Eds.), Handbook of Sea Level Research. Wiley, pp. 470–499.

Kemp, A.C., Horton, B.P., Donnelly, J.P., Mann, M.E., Vermeer, M., Rahmstorf, S., 2011. Climate related sea-level variations over the past two millennia. Proc. Natl. Acad. Sci. 108 (27), 11017–11022.

Khan, N.S., Ashe, E., Shaw, T.A., Vacchi, M., Walker, J., Peltier, W.R., Kopp, R.E., Horton, B.P., 2015. Holocene relative sea-level changes from near-, intermediate-, and far-field locations. Curr. Clim. Chang. Rep. 1 (4), 247–262.

Kjerfve, B., 1994. Coastal Lagoons. Elsevier Oceanography Series 60, pp. 1–8.

Kopp, R.E., Simons, F.J., Mitrovica, J.X., Maloof, A.C., Oppenheimer, M., 2009. Probabilistic assessment of sea level during the last interglacial stage. Nature 462 (7275), 863–867.

Laborel, J., Laborel-Deguen, F., 1994. Biological indicators of relative sea-level variations and of co-seismic displacements in the Mediterranean region. J. Coast. Res. 395-415.

Laborel, J., Morhange, C., Lafont, R., Le Campion, J., Laborel-Deguen, F., Sartoretto, S., 1994. Biological evidence of sea-level rise during the last 4500 years on the rocky coasts of continental southwestern France and Corsica. Mar. Geol. 120 (3), 203–223.

Lachenal, A.-M., 1989. Écologie des ostracodes du domaine méditerranéen: application au Golfe de Gabès (Tunisie orientale). Les variations du niveau marin depuis 30,000 ans. Documents des laboratoires de géologie de Lyon 108, pp. 1–239.

Lakhdar, R., Soussi, M., Ben Ismail, M.H., M'Rabet, A., 2006. A Mediterranean Holocene restricted coastal lagoon under arid climate: case of the sedimentary record of Sabkha Boujmel (SE Tunisia). Palaeogeogr. Palaeoclimatol. Palaeoecol. 241 (2), 177–191.

Lambeck, K., Bard, E., 2000. Sea-level change along the French Mediterranean coast for the past 30 000 years. Earth Planet. Sci. Lett. 175 (3), 203–222.

Lambeck, K., Purcell, A., 2005. Sea-level change in the Mediterranean Sea since the LGM: model predictions for tectonically stable areas. Quat. Sci. Rev. 24 (18), 1969–1988.

Lambeck, K., Antonioli, F., Purcell, A., Silenzi, S., 2004a. Sea-level change along the Italian coast for the past 10,000 yr. Quat. Sci. Rev. 23 (14), 1567–1598.

Lambeck, K., Anzidei, M., Antonioli, F., Benini, A., Esposito, A., 2004b. Sea level in Roman time in the Central Mediterranean and implications for recent change. Earth Planet. Sci. Lett. 224 (3), 563–575.

Lambeck, K., Antonioli, F., Anzidei, M., Ferranti, L., Leoni, G., Scicchitano, G., Silenzi, S., 2011. Sea level change along the Italian coast during the Holocene and projections for the future. Quat. Int. 232 (1), 250–257.

Lambeck, K., Rouby, H., Purcell, A., Sun, Y., Sambridge, M., 2014. Sea level and global ice volumes from the Last Glacial Maximum to the Holocene. Proc. Natl. Acad. Sci. 111 (43), 15296–15303.

Marco-Barba, J., Holmes, J.A., Mesquita-Joanes, F., Miracle, M.R., 2013. The influence of climate and sea-level change on the Holocene evolution of a Mediterranean coastal lagoon: evidence from ostracod palaeoecology and geochemistry. Geobios 46 (5), 409–421.

Marcos, M., Tsimplis, M.N., Shaw, A.G., 2009. Sea level extremes in southern Europe. J. Geophys. Res. Oceans (C1), 114.

Marra, F., Bozzano, F., Cinti, F.R., 2013. Chronostratigraphic and lithologic features of the Tiber River sediments (Rome, Italy): implications on the post-glacial sea-level rise and Holocene climate. Glob. Planet. Chang. 107, 157–176.

Marriner, N., Morhange, C., 2007. Geoscience of ancient Mediterranean harbours. Earth Sci. Rev. 80 (3), 137–194.

Marriner, N., Flaux, C., Morhange, C., Kaniewski, D., 2012a. Nile Delta's sinking past: quantifiable links with Holocene compaction and climate-driven changes in sediment supply? Geology 40 (12), 1083–1086.

Marriner, N., Gambin, T., Djamali, M., Morhange, C., Spiteri, M., 2012b. Geoarchaeology of the Burmarrad ria and early Holocene human impacts in western Malta. Palaeogeogr. Palaeoclimatol. Palaeoecol. 339, 52–65.

Marriner, N., Morhange, C., Faivre, S., Flaux, C., Vacchi, M., Miko, S., Rossi, I.R., 2014. Post-Roman sea-level changes on Pag Island (Adriatic Sea): dating Croatia's "enigmatic" coastal notch? Geomorphology 221, 83–94.

Maselli, V., Trincardi, F., 2013. Man made deltas. Sci. Rep. 3.

Mastronuzzi, G., Sanso, P., 2002. Holocene uplift rates and historical rapid sea-level changes at the Gargano promontory, Italy. J. Quat. Sci. 17 (5-6), 593–606.

Mastronuzzi, G., Sansò, P., 2012. The role of strong earthquakes and tsunami in the Late Holocene evolution of the Fortore River coastal plain (Apulia, Italy): a synthesis. Geomorphology 138 (1), 89–99.

Mauz, B., Ruggieri, G., Spada, G., 2015a. Terminal Antarctic melting inferred from a far-field coastal site. Quat. Sci. Rev. 116, 122–132.

Mauz, B., Vacchi, M., Green, A., Hoffmann, G., Cooper, A., 2015b. Beachrock: a tool for reconstructing relative sea level in the far-field. Mar. Geol. 362, 1–16.

Mazzini, I., Anadon, P., Barbieri, M., Castorina, F., Ferreli, L., Gliozzi, E., Mola, M., Vittori, E., 1999. Late Quaternary sea-level changes along the Tyrrhenian coast near Orbetello (Tuscany, central Italy): palaeoenvironmental reconstruction using ostracods. Mar. Micropaleontol. 37 (3), 289–311.

McClennen, C.E., Housley, R.A., 2006. Late-Holocene channel meander migration and mudflat accumulation rates, lagoon of Venice, Italy. J. Coast. Res. 930–945.

Micallef, A., Foglini, F., Le Bas, T., Angeletti, L., Maselli, V., Pasuto, A., Taviani, M., 2013. The submerged paleolandscape of the Maltese Islands: morphology, evolution and relation to Quaternary environmental change. Mar. Geol. 335, 129–147.

Milli, S., D'Ambrogi, C., Bellotti, P., Calderoni, G., Carboni, M.G., Celant, A., Di Bella, L., Di Rita, F., Frezza, V., Magri, D., Pichezzi, R.M., Ricci, V., 2013. The transition from wave-dominated estuary to wave-dominated delta: the Late Quaternary stratigraphic architecture of Tiber River deltaic succession (Italy). Sediment. Geol. 284, 159–180.

Milne, G.A., Mitrovica, J.X., 1998. Postglacial sea-level change on a rotating Earth. Geophys. J. Int. 133 (1), 1–19.

Milne, G.A., Mitrovica, J.X., 2008. Searching for eustasy in deglacial sea-level histories. Quat. Sci. Rev. 27 (25), 2292–2302.

Milne, G.A., Long, A.J., Bassett, S.E., 2005. Modeling Holocene relative sea-level observations from the Caribbean and South America. Quat. Sci. Rev. 24, 1183–1202.

Mitrovica, J.X., Milne, G.A., 2002. On the origin of late Holocene sea-level highstands within equatorial ocean basins. Quat. Sci. Rev. 21 (20), 2179–2190.

Morhange, C., Marriner, N., 2015. Archaeological and Biological Relative Sea-level Indicators. In: Shennan, I., Long, A., Horton, B.P. (Eds.), Handbook of Sea Level Research. Wiley, Wiley, pp. 146–156.

Morhange, C., Pirazzoli, P.A., 2005. Mid-Holocene emergence of southern Tunisian coasts. Mar. Geol. 220 (1), 205–213.

Morhange, C., Laborel, J., Hesnard, A., 2001. Changes of relative sea level during the past 5000 years in the ancient habour of Marseilles, Southern France. Palaeogeogr. Palaeoclimatol. Palaeoecol. 166 (3), 319–329.

Morhange, C., Marriner, N., Excoffon, P., Bonnet, S., Flaux, C., Zibrowius, H., Goiran, J., Amouri, M.E., 2013. Relative sea-level changes during Roman times in the northwest Mediterranean: the 1st century AD fish tank of Forum Julii, Fréjus, France. Geoarchaeology 28 (4), 363–372.

Morhange, C., Marriner, N., Laborel, J., Todesco, M., Oberlin, C., 2006. Rapid sea-level movements and noneruptive crustal deformations in the Phlegrean Fields Caldera, Italy. Geology 34 (2), 93–96.

Morri, C., Bellan-Santini, D., Giaccone, G., Bianchi, C.N., 2004. Principles of bionomy: definition of assemblages and use of taxonomic descriptors (macrobenthos). Biol. Mar. Mediterr. 11 (1), 573–600.

Nachite, D., Rodríguez-Lázaro, J., Martín-Rubio, M., Pascual, A., Bekkali, R., 2010. Distribution et écologie des associations d'ostracodes récents de l'estuaire de Tahadart (Maroc Nord-Occidental). Rev. Micropaléontol. 53 (1), 3–15.

Nelson, A.R., Shennan, I., Long, A.J., 1996. Identifying coseismic subsidence in tidal-wetland stratigraphic sequences at the Cascadia subduction zone of western North America. J. Geophys. Res. 101, 6115–6135.

Nesteroff, W.D., 1984. Étude de quelques grès de plage du sud de la Corse: datations ^{14}C et implications néotectoniques pour le bloc corso-sarde. Travaux de la Maison de l'Orient 8(1), pp. 99–111.

Neumeier, U. 1998. The role of microbial activity in early cementation of beachrocks (intertidal sediments). Unpublished PhD thesis, University of Geneva.

Nikula, R., Väinölä, R., 2003. Phylogeography of *Cerastoderma glaucum* (Bivalvia: Cardiidae) across Europe: a major break in the Eastern Mediterranean. Mar. Biol. 143 (2), 339–350.

Olivera, C., Susagna, T., Roca, A., Goula, X., 1992. Seismicity of the Valencia trough and surrounding areas. Tectonophysics 203 (1), 99–109.

Orrù, P.E., Antonioli, F., Lambeck, K., Verrubbi, V., 2004. Holocene sea-level change in the Cagliari coastal plain (southern Sardinia, Italy). Quaternaria Nova 8, 193–212.

Orrù, P.E., Mastronuzzi, G., Deiana, G., Pignatelli, C., Piscitelli, A., Solinas, E., Spanu, P., Zucca, R., 2014. Sea level changes and geoarchaeology between the bay of Capo Malfatano and Piscinnì Bay (SW Sardinia) in the last 4 kys. Quat. Int. 336, 180–189.

Orrù, P., Solinas, E., Puliga, G., Deiana, G., 2011. Palaeo-shorelines of the historic period, Sant'Antioco Island, south-western Sardinia (Italy). Quat. Int. 232 (1), 71–81.

Parnell, A.C., Gehrels, W.R., 2015. Using Chronological Models in Late Holocene Sea-level Reconstructions from Saltmarsh Sediments. In: Shennan, I., Long, A.J., Horton, Benjamin P. (Eds.), Handbook of Sea Level Research. Wiley, pp. 500–513.

Parnell, A.C., Buck, C.E., Doan, T.K., 2011. A review of statistical chronology models for high-resolution, proxy-based Holocene palaeoenvironmental reconstruction. Quat. Sci. Rev. 30 (21), 2948–2960.

Pedley, M., 2011. The Calabrian Stage, Pleistocene highstand in Malta: a new marker for unravelling the Late Neogene and Quaternary history of the islands. J. Geol. Soc. 168 (4), 913–926.

Pedoja, K., Husson, L., Johnson, M.E., Melnick, D., Witt, C., Pochat, S., Nexer, M., Delcaillau, B., Pinegina, T., Poprawski, Y., Authemayou, C., Elliot, M., Regard, V., Garestier, F., 2014. Coastal staircase sequences reflecting sea-level oscillations and tectonic uplift during the Quaternary and Neogene. Earth Sci. Rev. 132, 13–38.

Peltier, W.R., 2004. Global glacial isostasy and the surface of the ice-age earth: the ice-5G (VM2) model and grace. Annu. Rev. Earth Planet. Sci. 32, 111–149.

Peltier, W.R., Fairbanks, R.G., 2006. Global glacial ice volume and Last Glacial Maximum duration from an extended Barbados sea level record. Quat. Sci. Rev. 25 (23), 3322–3337.

Peltier, W.R., Tushingham, A.M., 1991. Influence of glacial isostatic adjustment on tide gauge measurements of secular sea level change. J. Geophys. Res. Solid Earth 96 (B4), 6779–6796.

Pérès, J.M., Picard, J., 1964. Nouveau manuel de bionomie benthique de la mer Méditerranée. Rech. Trav. Stat. Marit. Endoume 31, 1–137.

Pirazzoli, P.A., 1976. Sea level variations in the northwest Mediterranean during Roman times. Science 194 (4264), 519–521.

Pirazzoli, P.A., 2005. A review of possible eustatic, isostatic and tectonic contributions in eight late-Holocene relative sea-level histories from the Mediterranean area. Quat. Sci. Rev. 24 (18), 1989–2001.

Pirazzoli, P.A., Stiros, S.C., Arnold, M., Laborel, J., Laborel-Deguen, F., Papageorgiou, S., 1994. Episodic uplift deduced from Holocene shorelines in the Perachora Peninsula, Corinth area, Greece. Tectonophysics 229 (3), 201–209.

van de Plassche, O., 1982. Sea-level change and water-level movements in the Netherlands during the Holocene. Med. Rijks Geol. Dienst. 36, 1–93.

Preuss, H., 1979. Progress in Computer Evaluation of Sea Level Data within the IGCP Project no. 61. Proc. 1978 International Symposium of Coastal Evolution in the Quaternary, pp. 104–134.

Primavera, M., Simone, O., Fiorentino, G., Caldara, M., 2011. The palaeoenvironmental study of the Alimini Piccolo lake enables a reconstruction of Holocene sea-level changes in southeast Italy. The Holocene 21 (4), 553–563.
Raynal, O., Bouchette, F., Certain, R., Sabatier, P., Lofi, J., Seranne, M., Courp, T., 2010. Holocene evolution of a Languedocian lagoonal environment controlled by inherited coastal morphology (northern Gulf of Lions, France). Bull. Soc. Geol. Fr. 181 (2), 211–224.
Reimer, P., Reimer, R., 2001. A marine reservoir correction database and on-line interface. Radiocarbon 43, 461–463.
Reimer, P.J., Bard, E., Bayliss, A., Beck, J.W., Blackwell, P.G., Bronk Ramsey, C., Buck, C.E., Cheng, H., Edwards, R.L., Friedrich, M., Grootes, P.M., Guilderson, T.P., Haflidason, H., Hajdas, I., Hatta, C., Heaton, T.J., Hogg, A.G., Hughen, K.A., Kaiser, K.F., Kromer, B., Manning, S.W., Niu, M., Reimer, R.W., Richards, D.A., Scott, E.M., Southon, J.R., Turney, C.S.M., van der Plicht, J., 2013. IntCal13 andMARINE13 radiocarbon age calibration curves 0–50000 years cal BP. Radiocarbon 55http://dx.doi.org/10.2458/azu_js_rc.55.16947.
Reineck, H.E., Singh, I.B., 1973. Depositional Sedimentary Environments. FAO publishing.
Rossi, V., Amorosi, A., Sarti, G., Potenza, M., 2011. Influence of inherited topography on the Holocene sedimentary evolution of coastal systems: an example from Arno coastal plain (Tuscany, Italy). Geomorphology 135 (1), 117–128.
Rovere, A., Antonioli, F., Bianchi, C.N., 2015. Fixed Biological Indicators. In: Shennan, I., Long, A.J., Horton, B.P. (Eds.), Handbook of Sea Level Research. Wiley, pp. 268–280.
Rovere, A., Parravicini, V., Vacchi, M., Montefalcone, M., Morri, C., Bianchi, C.N., Firpo, M., 2010. Geo-environmental cartography of the marine protected area "Isola di Bergeggi"(Liguria, NW Mediterranean Sea). J. Maps 6 (1), 505–519.
Rovere, A., Vacchi, M., Firpo, M., Carobene, L., 2011. Underwater geomorphology of the rocky coastal tracts between Finale Ligure and Vado Ligure (western Liguria, NW Mediterranean Sea). Quat. Int. 232 (1), 187–200.
Ruiz, F., Abad, M., Bodergat, A.M., Carbonel, P., Rodríguez-Lázaro, J., Yasuhara, M., 2005. Marine and brackish-water ostracods as sentinels of anthropogenic impacts. Earth Sci. Rev. 72 (1), 89–111.
Ruiz, F., Abad, M., Galán, E., González, I., Aguilá, I., Olías, M., Goméz Ariza, G.L., Cantano, M., 2006. The present environmental scenario of El Melah Lagoon (NE Tunisia) and its evolution to a future sabkha. J. Afr. Earth Sci. 44 (3), 289–302.
Sabatier, P., Dezileau, L., Barbier, M., Raynal, O., Lofi, J., Briqueu, L., Condomines, M., Bouchette, F., Certain, R., Van Grafenstein, U., Jorda, C., Blanchemanche, P., 2010. South of France. Bull. Soc. Geol. Fr. 181 (1), 27–36.
Sacchi, M., Molisso, F., Pacifico, A., Vigliotti, M., Sabbarese, C., Ruberti, D., 2014. Late-Holocene to recent evolution of Lake Patria, South Italy: an example of a coastal lagoon within a Mediterranean delta system. Glob. Planet. Chang. 117, 9–27.
Sammari, C., Koutitonsky, V.G., Moussa, M., 2006. Sea level variability and tidal resonance in the Gulf of Gabes, Tunisia. Cont. Shelf Res. 26 (3), 338–350.
Sarti, G., Centineo, M.C., Calabrese, L., 2009. Carta Geologica d'Italia alla scala 1:50.000. Foglio 205, Comacchio. Note illustrative. http://www.isprambiente.gov.it/Media/carg/note_illustrative/205_Comacchio.pdf
Sartoretto, S., Verlaque, M., Laborel, J., 1996. Age of settlement and accumulation rate of submarine "coralligène"(−10 to −60 m) of the northwestern Mediterranean Sea; relation to Holocene rise in sea level. Mar. Geol. 130 (3), 317–331.
Schembri, P.J., Deidun, A., Mallia, A., Mercieca, L., 2005. Rocky shore biotic assemblages of the Maltese Islands (Central Mediterranean): a conservation perspective. J. Coast. Res. 157–166.
Schmiedt, G., 1972. Il livello antico del mar Tirreno. Testimonianze da resti archeologici. E. Olschki, Florence.
Scicchitano, G., Antonioli, F., Berlinghieri, E.F.C., Dutton, A., Monaco, C., 2008. Submerged archaeological sites along the Ionian coast of southeastern Sicily (Italy) and implications for the Holocene relative sea-level change. Quat. Res. 70 (1), 26–39.
Scicchitano, G., Monaco, C., Tortorici, L., 2007. Large boulder deposits by tsunami waves along the Ionian coast of south-eastern Sicily (Italy). Mar. Geol. 238 (1), 75–91.
Scicchitano, G., Spampinato, C.R., Ferranti, L., Antonioli, F., Monaco, C., Capano, M., Lubritto, C., 2011. Uplifted Holocene shorelines at Capo Milazzo (NE Sicily, Italy): evidence of co-seismic and steady-state deformation. Quat. Int. 232 (1), 201–213.
Serandrei-Barbero, R., Albani, A., Donnici, S., Rizzetto, F., 2006. Past and recent sedimentation rates in the Lagoon of Venice (Northern Italy). Estuar. Coast. Shelf Sci. 69 (1), 255–269.
Serpelloni, E., Faccenna, C., Spada, G., Dong, D., Williams, S.D., 2013. Vertical GPS ground motion rates in the Euro-Mediterranean region: new evidence of velocity gradients at different spatial scales along the Nubia–Eurasia plate boundary. J. Geophys. Res. Solid Earth 118 (11), 6003–6024.
Shennan, I., 1986. Flandrian sea-level changes in the Fenland. II: tendencies of sea-level movement, altitudinal changes, and local and regional factors. J. Quat. Sci. 1 (2), 155–179.
Shennan, I., Horton, B., 2002. Holocene land- and sea-level changes in Great Britain. J. Quat. Sci. 17, 511–526.
Shennan, I., Long, A.J., Horton, B.P., 2015. Handbook of Sea-Level Research. John Wiley & Sons.
Shennan, I., Milne, G., Bradley, S., 2012. Late Holocene vertical land motion and relative sea level changes: lessons from the British Isles. J. Quat. Sci. 27 (1), 64–70.
Silvestri, S., Defina, A., Marani, M., 2005. Tidal regime, salinity and salt marsh plant zonation. Estuar. Coast. Shelf Sci. 62 (1), 119–130.
Somoza, L., Barnolas, A., Arasa, A., Maestro, A., Rees, J.G., Hernández-Molina, F.J., 1998. Architectural stacking patterns of the Ebro delta controlled by Holocene high-frequency eustatic fluctuations, delta-lobe switching and subsidence processes. Sediment. Geol. 117 (1), 11–32.
Spada, G., Stocchi, P., 2007. SELEN: a Fortran 90 program for solving the "sea-level equation". Comput. Geosci. 33 (4), 538–562.
Spampinato, C.R., Costa, B., Di Stefano, A., Monaco, C., Scicchitano, G., 2011. The contribution of tectonics to relative sea-level change during the Holocene in coastal south-eastern Sicily: new data from boreholes. Quat. Int. 232 (1), 214–227.
Stiros, S.C., Pirazzoli, P.A., 2008. Direct determination of tidal levels for engineering applications based on biological observations. Coast. Eng. 55 (6), 459–467.
Stocchi, P., Spada, G., 2009. Influence of glacial isostatic adjustment upon current sea level variations in the Mediterranean. Tectonophysics 474 (1), 56–68.
Stocchi, P., Colleoni, F., Spada, G., 2009. Bounds on the time–history and Holocene mass budget of Antarctica from sea-level records in SE Tunisia. Pure Appl. Geophys. 166 (8-9), 1319–1341.
Strasser, A., Davaud, E., Jedoui, Y., 1989. Carbonate cements in Holocene beachrock: example from Bahiret et Biban, southeastern Tunisia. Sediment. Geol. 62 (1), 89–100.
Stuiver, M., Polach, H.A., 1977. Reporting ^{14}C data. Radiocarbon 19, 355–363.
Tornqvist, T.E., Rosenheim, B.E., Hu, P., Fernandez, A.B., 2015. Radiocarbon dating and calibration. In: Long, A.J., Horton, B.P. (Eds.), Shennan, I. Wiley, Handbook of Sea-level Research, pp. 349–360.
Törnqvist, T.E., Wallace, D.J., Storms, J.E.A., Wallinga, J., Van Dam, R.L., Blaauw, M., Derksen, M.S., Klerks, C.J.W., Meijneken, C., Snijders, E.M.A., 2008. Mississippi Delta subsidence primarily caused by compaction of Holocene strata. Nat. Geosci. 1, 173–176.
Tortorici, G., Bianca, M., de Guidi, G., Monaco, C., Tortorici, L., 2003. Fault activity and marine terracing in the Capo Vaticano area (southern Calabria) during the Middle–Late Quaternary. Quat. Int. 101, 269–278.
Triantaphyllou, M.V., Tsourou, T., Koukousioura, O., Dermitzakis, M.D., 2005. Foraminiferal and ostracod ecological patterns in coastal environments of SE Andros Island (Middle Aegean Sea, Greece). Rev. Micropaléontol. 48 (4), 279–302.
Tsimplis, M.N., Proctor, R., Flather, R.A., 1995. A two-dimensional tidal model for the Mediterranean Sea. J. Geophys. Res. Oceans 100 (C8), 16223–16239.
Vacchi, M., Rovere, A., Schiaffino, C.F., Ferrari, M., 2012a. Monitoring the effectiveness of re-establishing beaches artificially: methodological and practical insights into the use of video transects and SCUBA-operated coring devices. Underw. Technol. 30 (4), 201.
Vacchi, M., Rovere, A., Zouros, N., Desruelles, S., Caron, V., Firpo, M., 2012b. Spatial distribution of sea-level markers on Lesvos Island (NE Aegean Sea): evidence of differential relative sea-level changes and the neotectonic implications. Geomorphology 159, 50–62.
Vacchi, M., Rovere, A., Chatzipetros, A., Zouros, N., Firpo, M., 2014. An updated database of Holocene relative sea level changes in NE Aegean Sea. Quat. Int. 328, 301–310.
Vella, C., Provansal, M., 2000. Relative sea-level rise and neotectonic events during the last 6500 yr on the southern eastern Rhône delta, France. Mar. Geol. 170 (1), 27–39.
Vella, C., Fleury, T.J., Raccasi, G., Provansal, M., Sabatier, F., Bourcier, M., 2005. Evolution of the Rhône delta plain in the Holocene. Mar. Geol. 222, 235–265.
Vött, A., 2007. Relative sea level changes and regional tectonic evolution of seven coastal areas in NW Greece since the mid-Holocene. Quat. Sci. Rev. 26 (7), 894–919.
Vousdoukas, M.I., Velegrakis, A.F., Plomaritis, T.A., 2007. Beachrock occurrence, characteristics, formation mechanisms and impacts. Earth Sci. Rev. 85 (1), 23–46.
Zaîbi, C., Carbonel, P., Kamoun, F., Azri, C., Kharroubi, A., Kallel, N., Jedoui, Y., Montacer, M., Fontugne, M., 2011. Évolution du trait de côte à l'Holocène supérieur dans la Sebkha El-Guettiate de Skhira (Golfe de Gabès, Tunisie) à travers sa faune d'ostracodes et de foraminifères. Geobios 44 (1), 101–115.